TITLE Disordered clusters of Bak dimers rupture mitochondria during apoptosis

ARTICLE HIGHLIGHTS

- Bak dimers have very mobile, solvent-exposed N-termini, while the structured core and flexible C-termini are membrane-anchored.
- Interdimer interactions are weaker than the intradimer interaction.
- Bak dimer assembly is dynamic and lipid-mediated.
- Bak dimers aggregate in compact, disordered clusters to disrupt the mitochondrial outer membrane.

eTOC Blurb: The closely related proteins Bak and Bax are key mediators of apoptotic cell death. Here we present biochemical data and mathematical modelling that redefine how Bak dimers assemble at the molecular level to perforate the mitochondrial outer membrane.

AUTHORS/AFFILIATIONS

Rachel T. Uren[1,2], Martin O'Hely[1,2,3], Sweta Iyer[1,2], Ray Bartolo[1,4], Jason M. Brouwer[1,2], Amber E. Alsop[1,2], Grant Dewson[1,2], Ruth M. Kluck*[1,2].

1. The Walter and Eliza Hall Institute of Medical Research, 1G Royal Parade, Parkville, Victoria, 3052, Australia

2. Department of Medical Biology, The University of Melbourne, 1G Royal Parade, Parkville, Victoria, 3052, Australia

3. MOH Current address: Barwon Infant Study, Deakin University, PO Box 218, Geelong, Victoria, 3220, Australia

4. RB Current address: Murdoch Children's Research Institute, The Royal Children's Hospital, Flemington Road, Parkville, Victoria, 3052, Australia

CONTACT

* Corresponding author Ruth M. Kluck, The Walter and Eliza Hall Institute of Medical Research, 1G Royal Parade, Parkville, Victoria, 3052, Australia, Tel: +61 3 9345 2487; Fax: +61 3 9347 0852; Email: kluck@wehi.edu.au

SUMMARY

During apoptosis, Bak and Bax undergo major conformational change and form symmetric dimers that coalesce to perforate the mitochondrial outer membrane via an unknown mechanism. We have employed cysteine labelling and linkage analysis to the full length of Bak in mitochondria. This comprehensive survey showed that in each Bak dimer the N-termini are fully solvent-exposed and mobile, the core is highly structured, and the C-termini are flexible but restrained by their contact with the membrane. Dimer-dimer interactions were more labile than the BH3:groove interaction within dimers, suggesting there is no extensive protein interface between dimers. In addition, linkage in the mobile Bak N-terminus (V61C) specifically quantified association between dimers, allowing mathematical simulations of dimer aggregation. Together, our biochemical data and mathematical modelling show that Bak dimers form disordered, compact clusters to generate lipidic pores. These findings provide a molecular explanation for the observed structural heterogeneity of the apoptotic pore.

INTRODUCTION

The Bcl-2 family of proteins are the principal regulators of apoptotic cell death, with either Bak or Bax required to permeabilise the mitochondrial outer membrane (Lindsten et al., 2000, Wei et al., 2001). Bak and Bax are triggered to convert to their activated conformation by the binding of BH3-only relatives such as Bid and Bim (Gavathiotis et al., 2010, Dai et al., 2011, Du et al., 2011, Czabotar et al., 2013, Leshchiner et al., 2013, Brouwer et al., 2014), and once activated can be sequestered by pro-survival relatives such as Mcl-1 and Bcl-x_L (Llambi et al., 2011).

The ability of Bak and Bax to change conformation and oligomerize in the mitochondrial outer membrane appears crucial for their capacity to perforate this membrane (Westphal et al., 2014). Both proteins comprise nine α-helices that adopt a globular fold in the non-activated state (Suzuki et al., 2000, Moldoveanu et al., 2006). Non-activated Bak is anchored in the mitochondrial outer

membrane via the α9-helix forming a transmembrane domain (Iyer et al., 2015). In contrast, non-activated Bax is largely cytosolic due to binding of α9 to its own hydrophobic groove (Wolter et al., 1997, Gahl et al., 2014). Following binding of BH3-only proteins, both Bak and Bax undergo similar conformation changes including α1 dissociation (Weber et al., 2013, Alsop et al., 2015) and separation of the "latch" domain (α6-α8) from the "core" domain (α2-α5) (Czabotar et al., 2013, Brouwer et al., 2014). The core and α6 then collapse onto the membrane surface and become shallowly inserted into the membrane to lie in-plane (Aluvila, 2014, Bleicken et al., 2014, Westphal et al., 2014). Symmetric homodimers then form when the exposed BH3 domain of each molecule is re-buried in the hydrophobic groove of another activated molecule (Dewson et al., 2008, Dewson et al., 2012, Czabotar et al., 2013, Brouwer et al., 2014). Bax oligomers may also form prior to membrane insertion (Luo et al., 2014, Sung et al., 2015).

How symmetric homodimers of Bak or Bax then associate to porate the mitochondrial outer membrane is still unknown. Although there is structural information for Bak and Bax homodimers, no structures of higher order oligomers of Bak or Bax have been resolved. Bak and Bax have been shown to coalesce into clusters at the mitochondria upon an apoptotic stimulus (Nechushtan et al., 2001) and small clusters of Bax have been implicated in the rapid release of cytochrome *c* (Zhou and Chang, 2008). The availability of full-length recombinant Bax makes biochemical assays more amenable for Bax than for Bak. Thus, various oligomeric states of Bax have recently been detected with fluorescence and electron microscopy of recombinant Bax on artificial membranes (Subburaj et al., 2015, Kuwana et al., 2016). Furthermore, super-resolution microscopy has shown Bax can be found in ring-like structures, arcs and clusters at the mitochondrial outer membrane of apoptotic cells (Grosse et al., 2016, Salvador-Gallego et al., 2016), although the orientation of Bax dimers in these structures could not be visualised. Higher order oligomers of both Bak and Bax vary in size when assessed by gel filtration, blue native PAGE or linkage (George et al., 2007, Dewson et al., 2012). Moreover, linkage studies have identified several points at which dimers might associate, including interactions at α-helices 1, 3, 5, 6, and 9 (Dewson et al., 2008, Dewson et al., 2009, Zhang

et al., 2010, Pang et al., 2012, Ma et al., 2013, Aluvila, 2014, Bleicken et al., 2014, Gahl et al., 2014, Iyer et al., 2015, Zhang et al., 2016). Critically, it is not clear whether any of these interaction sites are required for dimer-dimer association and assembly of the apoptotic pore. Here, we address dimer assembly by comparison of linkages through the full length of Bak in cells and show that dimers associate in a disordered, lipid-mediated fashion.

RESULTS

The Bak N-segment, α1 and α1- α2 loop are solvent-exposed in Bak oligomers

To resolve how Bak dimers coalesce to porate the mitochondrial outer membrane, we sought to generate a more detailed biochemical map of the membrane topology of Bak dimers. This work complemented our previous cysteine-accessibility analyses of Bak α5, α6 and α9 (Westphal et al., 2014, Iyer et al., 2015), by analyzing the Bak N-terminus and additional residues in the α2-α5 core and C-terminus. The two native cysteine residues of human Bak (C14 and C166) were first substituted with serine to generate Bak Cys null (BakΔCys, i.e. C14S/C166S), and then a single cysteine residue substituted at several positions throughout the molecule. Each Bak variant was stably expressed in *Bak*$^{-/-}$*Bax*$^{-/-}$ mouse embryonic fibroblasts (MEFs) and tested for function (Figure S1). To convert Bak to the activated oligomeric form, membrane fractions enriched for mitochondria were incubated with tBid, as previously (Dewson et al., 2008). To label solvent-exposed cysteine residues, membrane fractions were treated with the thiol-specific labelling reagent IASD (4-acetamido-4'-((iodoacetyl) amino)stilbene-2,2'-disulfonic acid). Two negative sulfonate charges prevent IASD from accessing cysteine in hydrophobic environments (such as the mitochondrial outer membrane or the hydrophobic protein core), and also allow isoelectric focusing (IEF) to resolve IASD-labelled and IASD-unlabelled Bak (Tran et al., 2013, Westphal et al., 2014). We assessed each cysteine-substituted Bak variant for labelling before, during or after incubation with recombinant tBid or tBid^{Bax}, a tBid variant containing the Bax BH3 domain (Hockings et al., 2015), that activates Bak analogous to tBid, as well as a control not exposed to IASD and another

fully exposed to labelling by denaturation and membrane solubilization (Figure 1A, Figure S2). The approach thus monitors solvent-exposure of the residue as non-activated Bak converts to oligomeric Bak, and may detect transient exposure during these conformational changes.

In the N-terminus, most tested residues were accessible to IASD even before tBid treatment (Figure 1B and S2), consistent with the crystal structure (2IMT) (Moldoveanu et al., 2006). Two residues in α1 (R36C and Y41C) that were not fully accessible before tBid treatment became exposed following incubation with tBid (Figures 1B and S2). Two additional α1 residues, Q44C and Q47C, also showed a tendancy for increased labelling. These changes suggest that the α1-α2 loop separates from α1, consistent with increased labelling of A54C in the α1-α2 loop that opposes α1. Thus, increased labelling of cysteine residues placed throughout the N-segment, α1 and the α1-α2 loop, together with exposure of several N-terminal antibody epitopes (Alsop et al., 2015), indicate that the Bak N-terminus becomes completely solvent-exposed after activation (Figure 1D).

To complete our survey of the core and C-termini of Bak dimers (Westphal et al., 2014, Iyer et al., 2015), we tested the cysteine accessibility of additional selected residues in the α2-α5 core and the α7-α8 region (Figures 1B and S2). A summary of current and previous cysteine labelling data for the full length of the Bak protein in Figure 1C provides the following picture of Bak dimer topology. Certain cysteine residues placed in α2 became transiently exposed, consistent with exposure of the BH3 domain and then its burial in the hydrophobic groove in the α2-α5 core dimer (Figure 1C), as predicted by the published structure of the Bak BH3:groove homodimer (4U2V) (Brouwer et al., 2014). Cysteine substitutions on the exposed surface of α3 were successfully labelled with IASD before, during and after tBid treatment. In contrast, two buried residues in α4 were refractory to IASD labelling throughout. In the α4-α5 linker region, although I123C became more exposed following activation, it was still incompletely labelled. This may reflect loss of contact between I123C and two hydrophobic residues in the "latch" (I167 and W170), followed by shallow membrane insertion of I123C as it resides on the hydrophobic face of the Bak dimer core.

Partial labelling of this residue is consistent with shallow membrane insertion as IASD can label cysteine moieties up to 7.5 Å into the hydrocarbon core of a lipid bilayer (Grundling et al., 2000, Westphal et al., 2014). Within the C-termini, the profile of IASD-labelling was consistent with the amphipathic α6 helix lying in-plane on the membrane surface (Westphal et al., 2014) and the hydrophobic α9 forming the sole transmembrane domain (Figure 1D).

In summary, Bak undergoes a series of conformational changes as it transitions from its non-activated monomeric state, to an activated BH3-exposed monomeric intermediate, to the symmetric dimer that is the building block of the Bak oligomer (Figure 1D). In the course of these structural rearrangements, some regions of Bak display changes in solvent exposure (such as α1 which becomes more exposed, or α2 which is transiently exposed) whilst others remain buried throughout (such as the α9 transmembrane anchor).

The N- and C-termini of activated Bak are mobile

Linkage studies have provided significant insight into structural changes in Bak, as well as how the activated proteins associate into high order oligomers (Dewson et al., 2008, Dewson et al., 2009, Ma et al., 2013, Aluvila, 2014, Brouwer et al., 2014, Iyer et al., 2015). To directly compare reported linkages, and to analyse the full length of Bak, we used our expanded library of single-cysteine Bak variants. Each substituted cysteine was tested for the ability to disulphide bond to the same residue in a neighbouring Bak molecule (or to a cysteine in a nearby protein) upon addition of the oxidant copper phenanthroline (CuPhe). Linkage between Bak molecules was indicated by the presence of 2x complexes corresponding to twice the molecular weight of the Bak monomer on non-reducing SDS-PAGE. (Note that in this manuscript, "dimer" refers only to the native BH3:groove dimer that forms even in the absence of linkage, as shown below on BNP.) This system of single cysteine substitutions offers an elegant screening approach for assessing the proximity of single cysteine residues in neighbouring molecules in a point-to-point manner, but does not identify interaction surfaces where a single cysteine substitution may not contact its counterpart (See Discussion).

Even in the absence of tBid treatment, cysteine residues in flexible regions displayed some linkage to neighbouring non-activated Bak molecules (Figure 2, upper panels). For example, some 2x complexes were captured by cysteine substitutions in the flexible N-segment (G4C, C14, L19C, S23C), and α1-α2 loop (G51C, D57C, P58C, Q66C, S68C, S69C), indicating some proximity of Bak monomers in untreated mitochondria. Furthermore, disulphide linkage to proteins other than Bak resulted in Bak complexes larger than the 2x species and was observed for cysteine substitutions in the α2-α3 helices (D84C, R87C), α4-α5 loop (S121C, N124C), α8-α9 linker (G186C, I188C) and C-terminal end of α9 (V205C). This is unsurprising as the MOM is a protein-rich environment and there are documented examples of monomeric Bak associating with other membrane proteins such as VDAC2 (Cheng et al., 2003, Lazarou et al., 2010, Ma et al., 2014).

After addition of tBid had activated Bak, each cysteine in the N-extremity (a region comprising the N-terminus, α1 and α1-α2 loop) showed more efficient linkage to 2x complexes (Figure 2A, upper panel). The freedom with which each cysteine in the N-extremity of Bak can link suggests this region is highly mobile and does not engage in stable protein-protein or protein-lipid interactions following activation. In contrast, cysteine residues positioned in the core (α2-α5) showed relatively modest linkage to 2x complexes (Figure 2B, upper panel), consistent with lack of flexibility in the α2-α5 core dimer (Brouwer et al., 2014) and its relative immobility due to association with the membrane.

We next addressed linkage in the C-extremity encompassing the α6-α8 latch and α9 transmembrane domain (Figure 2C, upper panel). After Bak activation, H164C in α6 showed increased linkage to 2x complexes, as reported previously (Dewson et al., 2009, Ma et al., 2013). Cysteine substitutions in the α8-α9 loop and the beginning of the α9 transmembrane domain (up to residue N190C) also showed linkage to 2x complexes (Figure 2C, upper panel). However, compared to the N-extremity, linkage was less complete, possibly due to membrane association limiting mobility. Linkage of membrane-buried α9 residues was even less efficient (Figure 2C). However, at a higher temperature

α9 residues show much stronger linkage (Figure S3) (Iyer et al., 2015), attributable to increased Bak mobility or CuPhe penetration into the bilayer.

In summary, after Bak activation, the whole N-extremity is highly dynamic due to being fully solvent-exposed; the core is constrained and membrane-associated; and the C-extremity is flexible, but is anchored to the membrane.

Mobility of the N- and C-extremities permits linkage between dimers

We next used blue native PAGE (BNP) to consider two types of cysteine-mediated Bak linkage: linkage *within* Bak dimers and linkage *between* Bak dimers. The Bak BH3:groove interaction *within* dimers is an extensive protein-protein interface and is stable in 1% digitonin on BNP while the interaction between dimers is not (Ma et al., 2013). Thus oligomerized Bak migrates only as BH3:groove dimers on BNP. Addition of CuPhe to mitochondrial extracts prior to BNP can stabilise high order complexes on BNP and does so by cysteine-mediated linkage *between* dimers (Ma et al., 2013). Thus, if addition of CuPhe at the end of the mitochondrial incubation generated 4x and greater complexes on BNP, we conclude that the linkage was *between* dimers. If larger complexes were absent and dimers predominated on BNP, any linkage was *within* the dimer. Thus, parallel examination of CuPhe linked Bak species on BNP and non-reducing SDS PAGE permits differentiation of three conditions: linkage *within* the dimer, linkage *between* dimers, or no cysteine linkage (Figure 3A).

In the N-extremity (G4C to S69C), each introduced cysteine could link some dimers to larger complexes on BNP (Figure 2A, lower panel). Upon tBid activation, SDS-PAGE showed an increased proportion of 2x complexes, and higher order complexes (>10x) were observed on BNP for all residues. Of note was a stretch of residues from E59 to T62 that, following tBid treatment, exhibited very efficient linkage by SDS-PAGE (obvious 2x, negligible 1x). In this stretch, BNP showed no dimer species and a concomitant shift to 4x species and higher order complexes,

indicating efficient linkage between dimers but no linkage within dimers. Residues closer to the α2-α5 core (Q66C to S69C), showed progressively more 1x species (SDS-PAGE) and an increase in dimers (BNP), indicative of becoming closer to the constrained core of the dimer. Together, these linkage data further argue that dimers possess flexible N-extremities capable of efficient linkage within and between dimers, with linkage becoming exclusively between dimers as residues approach the constrained α2-α5 core (Figure 3B). Interestingly, because linkage of cysteine residues in the E59-T62 region occurs *only* between dimers, and is very efficient, this linkage provides a molecular sensor that can specifically quantitate dimer-dimer interactions, and is the first assay to do so.

In the Bak C-terminus also, cysteines could link dimers to larger complexes on BNP, although a striking laddering pattern was apparent (Figure 2C, lower panels). For example, the large (>10x) complexes common at the highly mobile N-extremity were not apparent at the membrane-associated C-extremity. Stronger ladders for certain residues may be explained by the membrane associated α6-α8 allowing only certain residues to be presented laterally. Lastly, linkage in the C-extremity may be only between dimers (rather than within dimers) as the proportion of 2x to 1x species on SDS-PAGE is similar to the proportion of high order complexes to dimers on BNP.

Single-cysteine mutants in the rigid core capture some linkage, mostly at the lateral edges

Previous studies suggested that the structured α2-α5 core of the Bak (or Bax) dimer might form a dominant, symmetric interface capable of driving dimers to form higher order complexes (Aluvila, 2014, Brouwer et al., 2014). For example, crystals of the Bak α2-α5 core dimer showed a side-by-side association (4U2V)(Brouwer et al., 2014). However, this was attributed to crystal packing effects, as chemical crosslinking between the α4-α5 loops was not detected (Brouwer et al., 2014). Accordingly, in the present studies, disulphide bonding between the α4-α5 loops was not captured with CuPhe (Figure 2B, lower). End-to-end associations were suggested by α3:α3' or α5:α5' linkages (Aluvila, 2014, Brouwer et al., 2014), and disulphide bonding at the equivalent residues

was also evident in this study (H99C:H99C for α3:α3'; H145C:H145C' for α5:α5')(Figure 2B, lower). Notably, this linkage was not as efficient as linkage observed for the N-extremity, and these and other linkage-competent residues locate mostly to the lateral edges of the α2-α5 core dimer when lying in-plane (Figure 3C). Thus, screening individual cysteine substitutions in the Bak dimer core for linkage did not uncover any dominant sites of interaction between Bak dimers, but showed widespread linkage of residues around the lateral edges of the dimer, consistent with the random collision of Bak dimers.

These findings support a flexible extremity model for full-length Bak dimers in the MOM, outlined in Figure 3D with side-on (left) and top-down views (right). At the centre is the α2-α5 core dimer lying in-plane and partially submerged in the membrane surface. Extending from both sides of the core dimer is a flexible latch (α6-α8) of ~50 residues that also lies in-plane and connects to the transmembrane α9-helices. Extending from both ends of the dimer core is the solvent-exposed, flexible and mobile N-extremity of ~70 residues. Each circle in Figure 3D illustrates the range of possible positions for the flexible N- and C-extremities (blue and pink respectively). Overlap of the largest blue circles (labelled G4C) indicates the potential for residues close to the N-terminus to link within dimers. In contrast, the smaller blue circles (labelled V61C) do not overlap, indicating a lack of linkage within the dimer at this residue. Notably, these linkage constraints are consistent with the dimensions of the α2-α5 dimer core as determined from the recent crystal structure (4U2V) (Figure 3E).

These findings also reveal how dimers associate into high order oligomers. As linkage can be induced between several regions of the Bak dimer, there is no dominant protein-protein interface that mediates dimer assembly into high order oligomers. Rather, the linkage pattern is consistent with transient collision of dimers in-plane on the membrane. Collisions of the α2-α5 core and α6-α8 latch are limited by their membrane-association, whereas the flexible, entirely solvent-exposed N-terminal region is free to link between dimers and does so very efficiently.

Inter-dimer interfaces are more labile to detergent than the intra-dimer (BH3:groove) interface

We next examined if the inter-dimer interactions identified above were stable in digitonin, as shown for the BH3:groove interface within dimers (Ma et al., 2013). Digitonin was added to the mitochondrial incubations after Bak had become oligomerized by incubation with tBid, but prior to disulphide bond formation induced by CuPhe (Figure 4A). As expected, digitonin did not prevent linkage *within* dimers as shown by 2x complexes of M71C/K113C on SDS-PAGE (Figure 4A, upper panel, lane 3). However, digitonin prevented all linkage *between* dimers on BNP of seven single-cysteine variants (Figure 4A, lower panel).

These experiments also provided new insight into linkage within dimers. For example, two residues at the far N- and C-termini (L19C and the C-terminal extension GGSGGCK (Iyer et al., 2015)) could link within dimers to generate 2x complexes on SDS-PAGE after digitonin treatment (Figure 4A, upper panel). Presumably, these residues were sufficiently distal from the core to reach their counterpart across the length of the structured α2-α5 core dimer and allow linkage within the dimer (Figure 3D, 3E). On BNP, dimers of these two residues (L19C, and to a lesser extent GGSGGCK) also migrated faster than dimers of other variants (Figure 4A, lower panel), suggesting that linkage within the dimer caused a more compact, faster migrating protein complex under these native conditions.

Bak dimers can become interspersed with Bax

To test if interactions between Bak dimers could be disrupted by other proteins, and thus test if Bak dimer aggregation was a dynamic, reversible process, we added recombinant proteins from the Bcl-2 protein family after Bak had formed dimers (Figure 4B). Dimer interactions were monitored by linkage between the N-termini (V61C:V61C') or C-termini (H164C:H164C'), and compared to BH3:groove linkage (M71C:K113C). To oligomerize Bak, mitochondria were first incubated with $tBid^{M97A}$, a variant that binds poorly to prosurvival proteins such as Bcl-x_L and Mcl-1 (Lee et al.,

2016). Mitochondria were then incubated with recombinant Bax, Bcl-x_L or Mcl-1ΔNΔC. Finally, CuPhe was applied and the extent of disulphide linkage assessed by non-reducing SDS-PAGE (Figure 4B). Notably, Bax translocated to mitochondria and decreased linkage between Bak dimers (e.g. V61C:V61C' and of H164C:H164C') but not within dimers (e.g. M71C:K113C) (Figure 4B). Thus, Bax appears not only to localise to the same region as the pre-formed Bak oligomers, but to become partially interspersed with the dimers. In contrast, recombinant Bcl-x_L and Mcl-1ΔNΔC also localised to the mitochondrial membrane but did not interfere with linkage between Bak dimers (Figure 4B).

V61C:V61C' linkage can monitor dimer-dimer interactions; stochastic simulation

To infer the probable architecture of the Bak apoptotic pore, we performed stochastic simulations based on V61C:V61C' linkage between the N-termini. As the V61C:V61C' linkage generates a distinct pattern of prominent 4x complexes and >10x complexes (Figure 5A, 5B), we considered which dimer-dimer arrangements would be consistent with this distinct linkage pattern. Simulation parameters allowed each dimer to make at most 2 cysteine linkages, but possibly only 1 or 0 linkages if no other free cysteines were available. The output was a frequency distribution of the number of Bak dimers present in each linked complex (Figure S4). To approximate the BNP western blot densitometry (Figure 5B), the counts were multiplied by the number of Bak dimer units (e.g. 1, 2, 3, 4 etc) in each of the linked Bak complexes, and the predicted densitometry smoothed with a gaussian kernel to allow qualitative comparison with the gaussian-like densitometry output from the BNP western blots (Figure S4).

One-dimensional modelling: testing a linear array of Bak dimers

We first simulated a simple one-dimensional (1D) arrangement in which Bak dimers interacted via a single (symmetric) interface between dimers (Figure 5C), as this arrangement is present in well-characterised pores (Song et al., 1996, Mueller et al., 2009). In addition, versions of this regular

architecture have recently been considered for Bak and Bax, either as a transverse array on the membrane surface (as per (Iyer et al., 2015)) or as a closed circuit of dimers lining a circular pore (as per (Aluvila, 2014, Bleicken et al., 2014, Brouwer et al., 2014)) (Figure 5C). Those reports also considered whether, within a linear array, dimers assembled side-by-side, end-to-end, or in a more oblique corner-to-corner arrangement (Figure 5C).

One-dimensional stochastic simulations were performed as described in Experimental Procedures. Alternative arrangements (e.g. side-to-side or end-to-end) were simulated by varying the ratio of *cis* to *trans* linkage (Figure 5D) from 1:0 to 0:1 (Figures 5E and S5). At a ratio of 0:1, when V61C:V61C' linkage occurred only between cysteine residues on opposite sides of the plane of symmetry (i.e. in trans), the output was Bak dimers that link endlessly and efficiently to very large oligomers (Figure 5E). This pattern clearly does not match the heterogeneous complexes observed with V61C:V61C' BNP linkage densitometry (Figure 5B). At a ratio of 1:0, when V61C:V61C' linkage was only permitted between cysteine residues on the same side of the array (i.e. in cis), the output was mostly tetramers with some higher order oligomers (Figure 5E), which again is a poor fit with the BNP densitometry (Figure 5B). In the intermediate examples where the ratio of cis to trans linkage was varied, the ratio of 0.5:0.5 (i.e. an equal mixture of cis and trans linkage) generated an output that very closely matched the complexes on BNP (Figures 5E and S5). If the maximum oligomer size was decreased from 10,000 dimers (to 50, 20, 10 or 6 dimers), the best fit was again seen with a ratio of 0.5:0.5 (Figure S5). Thus, 1D simulations showed best fit when there was an equal preference for cis and trans linkage, ruling out a side-by-side or end-to-end arrangement. Rather, the simulations are consistent with an oblique array of Bak dimers in which a hypothetical single dominant interface between dimers allows neighbouring cis and trans V61C residues to be equidistant (Figure 5E,cis 0.5, trans 0.5).

While the 1D simulations are consistent with an oblique arrangement of dimers (as in cis 0.5: trans 0.5, Figure 5E), our biochemical data do not support the existence of a single, dominant protein-

protein interface between dimers. An alternative interpretation of the good concordance between the model and the linkage data in the case of the cis 0.5: trans 0.5 linear simulation was that dimers adopt a random arrangement, but still within the linear array. When randomly orientated, dimers are not arranged with a plane of symmetry, and thus cis and trans linkages are equally likely. We note however, that if dimers arrange randomly in one dimension (e.g. linearly around the rim of a pore), they may also arrange randomly in two dimensions (e.g. as clusters on the surface of mitochondria). Indeed, several studies indicate that Bax and Bak can reside in a variety of different structures at the mitochondrial outer membrane of apoptotic cells, including clusters (Nechushtan et al., 2001, Zhou and Chang, 2008, Grosse et al., 2016, Nasu et al., 2016, Salvador-Gallego et al., 2016). Therefore, we next explored the possibility of a random dimer orientation not just in one dimension, but in two dimensions**.**

Two-dimensional simulation reveals a disordered aggregate of Bak dimers

To test if disordered clustering of Bak at the membrane would fit with our empirical data, we used 2D simulations in which Bak dimers were evenly distributed on a flat surface, with each dimer randomly oriented relative to its neighbours (Figure 6A). This simple simulation involved the even distribution of dimers on a geometric grid and, to avoid edge effects, the grid was wrapped onto a torus. A hexagonal grid was employed to represent the close packing of objects on a plane with the greatest degrees of freedom. Each Bak dimer was represented by a single unit hexagon, and each unit had the freedom to link (e.g. V61C:V61C') with at most two neighbouring hexagons, in any direction. This would result in a mixture of linkage states including double, single or no linkages. With this hexagonal grid, four types of double linkage were possible; opposite, obtuse, acute or reciprocal (Figure 6B).

Thus, in the simulations, we imposed an equal probability for each of the double linkages (opposite, obtuse, acute or reciprocal), to reflect close but random packing of dimers at the membrane. In addition, the simulation was allowed to proceed to complete linkage of available cysteine residues,

to reflect the tendency of disulphide bond formation to go to completion in the presence of CuPhe. With this simple set of assumptions, the simulation predicted a linkage pattern with prominent 4x complexes and >10x complexes (Figure 6C and 6D), which closely fitted the V61C:V61C' BNP linkage pattern in mitochondria (Figure 5B). Thus, simulation of random dimer linkage in 2 dimensions, as well as in 1 dimension, displayed a clear agreement with our empirical data, supporting a model of Bak dimers making random contacts with their near neighbours.

Two-dimensional simulations are robust to a reduction in linkage

To explore robustness in our 2D simulations, we performed mitochondrial experiments in which ~50% of the Bak molecules lacked cysteine residues. In those experiments, Bak V61C was co-expressed with Bak Cys-null that was FLAG-tagged (Figure S6A, upper panel). As expected, only half of the Bak molecules could link to 2x species after activation by tBid and induction of linkage (Figure S6A, middle panel, lane 4). In addition, all molecules formed BH3:groove dimers after incubation with tBid, as shown by BNP, but the capture of higher order oligomers mediated by cysteine-linkage was greatly reduced (Figure S6A, lower panel, lane 4; quantified in Figure S6B).

In simulations of this system, we assumed equal expression of V61C and the Cys null variants, as indicated by the western blot. We also assumed this population of monomers forms dimers in Mendelian proportions: 25% of dimers are V61C doublets and can link twice, 50% are V61C:Cys null and can link once, and the remaining 25% are Cys null doublets and cannot link (Figure S6C). The simulation output (Figure S6D) reflected that of the BNP densitometry (Figure S6B) in terms of more dimers and fewer >10x complexes, indicating robustness of the 2D simulations.

We next examined if our 2D simulations were also robust when approximating the pattern of linkage observed for residues other than V61C (Figure S7A). As noted above, because T62C, Q66C, S68C, and S69C substitutions were closer than V61C to the constrained α2-α5 core, they did not link efficiently (Figure 2A lower, quantified in Figure S7B). To simulate steric hindrance

imposed by proximity to the constrained core, an *edge blocking* effect was introduced; every edge of every hexagon was prohibited from having a link form across it with this probability for the duration of each simulation. As the edge blocking probability increased from 0 to 0.75, linkage between dimers decreased to generate patterns comparable to BNP analysis of these core-proximal residues (Figure S7C). Thus, 2D simulations based on simple sets of assumptions, support a model of random Bak dimer aggregation at the mitochondrial outer membrane, not only when based on V61C:V61C' linkage, but on other linkages that occur between Bak dimers when Bak permeabilizes the outer membrane.

DISCUSSION

Here we investigated the topology of Bak dimers in the mitochondrial outer membrane, and how dimers assemble into the high order oligomers thought necessary to form apoptotic pores in that membrane. We found that Bak dimers are characterized by flexible N- and C-extremities flanking a rigid α2-α5 core, and that these dimers aggregate in disordered, dynamic, compact clusters. Critically, we found no evidence for a single, dominant protein-protein interface between dimers and predict the lipid environment plays a crucial role in facilitating the aggregation of dimers and subsequent membrane rupture.

We had previously proposed the in-plane model for Bak dimers (Westphal et al., 2014). Our current data advances this model to show the N- and C-extremities are flexible, based on analysis of the full-length of Bak when activated and dimerised at the mitochondrial outer membrane (Figure 3D). The N-extremity (~70 residues C-terminal to α2) becomes fully solvent-exposed as shown by IASD labelling, and fully mobile as indicated by linkage, consistent with exposure of N-terminal cleavage sites and antibody epitopes in α1 and the α1-α2 loop (Griffiths et al., 1999, Weber et al., 2013, Alsop et al., 2015). Failure of the N-extremity to re-engage in protein-protein or protein-lipid interactions argues that it does not contribute to the assembly of dimers. The remainder of Bak is membrane-associated, with the α2-α5 core and α6 (and possibly α7-α8) in-plane with the outer

mitochondrial membrane surface and partially embedded (Aluvila, 2014, Brouwer et al., 2014, Westphal et al., 2014) while α9 forms a transmembrane domain (Iyer et al., 2015). The topology of the α2-α5 region is consistent with the α2-α5 core dimer crystal structure (~35Å × 45Å)(Brouwer et al., 2014), as V61C (~30Å from the core dimer) linked between dimers but not within dimers. Flexibility of the C-terminal α6-α9 region, as indicated by multiple linkages between these regions (Bleicken et al., 2014, Iyer et al., 2015, Zhang et al., 2016), implies that embedded dimers adopt a range of conformations on the MOM surface.

Linkage experiments have identified several possible interactions between dimers of Bak or Bax (Dewson et al., 2008, Dewson et al., 2009, Zhang et al., 2010, Pang et al., 2012, Ma et al., 2013, Aluvila, 2014, Bleicken et al., 2014, Gahl et al., 2014, Iyer et al., 2015, Zhang et al., 2016), with many evident in the present study. Notably, however, a dominant protein-protein interface between dimers was not evident. Rather, linkage between the membrane-associated regions could be detected at many positions, arguing for a disordered arrangement. As our single-cysteine scanning approach can only examine the homotypic pairing of cysteine residues, it remains possible that heterotypic pairing of cysteine substitutions may detect a more complex protein interface between dimers, as seen for near complete linkage at the Bak BH3:groove interface (M71C:K113C, Figure 4B) (Dewson et al., 2008). However, in support of the notion that there is no dominant protein interface between dimers, the interaction between Bak dimers is lost when digitonin is added, in contrast to the BH3:groove interface which persists in the presence of digitonin. Moreover, lability of dimer-dimer association was highlighted by the capacity of Bax to intermingle with pre-formed Bak dimers. Each of Bcl_{xL}, Mcl-1 and Bax localised to mitochondria with similar efficiency, however a critical feature of Bax is that is will form homodimers, and thus may contribute a greater area of displacement than the monomeric pro-survival proteins. This phenomenon may explain the greater efficiency with which Bax appeared to disrupt Bak dimer-dimer association in this assay.

A variety of biophysical and imaging techniques have been deployed to better understand how Bak (or Bax) dimers associate, yet it remains unclear. Here a novel and complementary approach of mathematical modelling was used to simulate linkage between Bak dimers and thus gain insight into dimer association. Since the V61C residue linked only between Bak dimers, and did so very efficiently, this provided a powerful tool for testing different arrangements of Bak dimers on the membrane. Our linkage assays capture the whole population of Bak at the membrane. As pores no longer form if Bak levels decrease by ~50% in MEFs (Ferrer et al., 2012), our observations from this whole population of Bak represent the species of Bak dimers responsible for pore formation, rather than a minor species not involved in pore formation. A minimalist set of assumptions were adopted for stochastic simulations of linkage between Bak dimers: linkage is complete and irreversible, but occurs only between dimers; only two linkages are possible per dimer; and neighbouring dimers can only link if both have a free cysteine available for disulphide bonding. One dimensional (1D) simulations in which Bak dimers interacted via a single dominant interface showed that the dimers would be neither side-by-side nor end-to-end, but would exhibit an oblique alignment because there was no clear preference for V61C:V61C' linkage in either the cis or trans orientation. Since our biochemical data revealed that there is no single dominant interface between the α2-α5 core dimers, we interpreted this lack of cis/trans preference as reflecting a random arrangement of dimers. Indeed, when this randomness was explored with 2D modelling, without the constraints of a linear array, the simulation showed good concordance with our linkage data. From this we conclude that Bak dimers are closely packed and aggregate with a random orientation.

A disordered cluster of dimers is reminiscent of the "carpet" model of pore formation by peptides (reviewed by (Gilbert, 2016)). Amphipathic antimicrobial peptides such as melittin accumulate on the membrane surface prior to their insertion across the membrane and pore formation (Lee et al., 2013). They also have membrane thinning attributes (Chen et al., 2003), as reported for Bax (Satsoura et al., 2012). Satsoura and colleagues discuss how membrane deformation by Bax may promote oligomerization mediated not by protein:protein interactions but by long-range changes in

membrane tension (Satsoura et al., 2012). Moreover, like an amphipathic peptide, the Bak and Bax α2-α5 core dimers and α6-helices penetrate the outer leaflet of the bilayer (Czabotar et al., 2013, Aluvila, 2014, Brouwer et al., 2014, Westphal et al., 2014). Thus, we hypothesize that lipidic pores may result from Bak dimers penetrating the outer leaflet to attract further dimers and in doing so increase the membrane disturbance. Enlarging clusters may then destabilize the membrane sufficiently to release apoptogenic factors (Figure 7). Subsequently, lipids and Bak dimers then rearrange to accommodate these drastic changes in membrane tension by burying exposed hydrophobic surfaces, thus stabilizing a variety of protein-lipid (toroidal) channels or "pores". Hence, our model for the disordered clustering of Bak dimers provides a holistic molecular explanation for the detection of Bax and Bak in a variety of formations including complete rings, arcs, lines and random clusters (Grosse et al., 2016, Kuwana et al., 2016, Nasu et al., 2016, Salvador-Gallego et al., 2016).

In conclusion, this study proposes a novel means of oligomerization by Bak and Bax in apoptotic cells: that dimers aggregate in dense clusters without a dominant interface and this dynamic association requires the involvement of the lipid membrane. We have described molecular tools that can precisely monitor the aggregation of Bak dimers in cells. These tools will greatly aid the further characterisation of the molecular events governing formation of the enigmatic "apoptotic pore" and how this process might be manipulated for therapeutic gain. More broadly, this study may have application to understanding the assembly of other unconventional pore-forming proteins.

EXPERIMENTAL PROCEDURES

Recombinant proteins

Recombinant proteins were prepared as previously described; caspase 8-cleaved human Bid (tBid) (as per (Kluck et al., 1999)), $tBid^{Bax}$ and Bcl-x_L full length (as per (Hockings et al., 2015)), Bax full

length (as per (Czabotar et al., 2013)), Mcl-1ΔN151ΔC23 (as per (Chen et al., 2005). $tBid^{M97A}$ was kindly provided by E. Lee (Lee et al., 2016).

Bak variant library cloning and expression

A library of human Bak mutants was generated by site-directed cysteine substitution (as per (Dewson et al., 2008). Human Bak with the endogenous cysteine residues mutated to serine (Bak Cys null C14S/C166S) was used as the template in overlap extension PCR to introduce single cysteine residues throughout the Bak sequence, and then cloned into the pMX-IRES-GFP retroviral vector (primer and vector sequences available on request). Mutants were introduced into SV40-immortalized *Bak*$^{-/-}$*Bax*$^{-/-}$ mouse embryonic fibroblasts (MEFs) by retroviral infection (as per (Dewson et al., 2008).

Preparation of membrane fractions enriched for mitochondria

Bak$^{-/-}$*Bax*$^{-/-}$ MEFs expressing Bak cysteine mutants were permeabilised and membrane fractions containing the mitochondria were isolated as previously described (Dewson et al., 2008). Cells were washed in PBS and then re-suspended at a concentration of 1×10^7 cells/ml in wash buffer supplemented with digitonin (100 mM sucrose, 20 mM HEPES-NaOH pH 7.5, 100 mM KCl, 2.5 mM $MgCl_2$, 4 μg/ml Pepstatin A (Sigma-Aldrich, St. Louis, MO, USA), Complete protease inhibitors (Roche, Castle Hill, NSW, Australia) and 0.025% w/v digitonin (Calbiochem, Merck, Darmstadt, Germany). Cells were incubated for 10 min on ice, then membrane fractions were collected by centrifugation at 16,000 ×*g* for 5 min and the supernatant discarded. Pellets were re-suspended in wash buffer (no digitonin), and permeabilisation of the cell membrane confirmed by trypan blue uptake.

Activation of Bak by tBid or Etoposide

To assess the apoptotic function of each Bak variant in cells, *Bak*$^{-/-}$*Bax*$^{-/-}$ MEFs expressing Bak cysteine mutants were treated with etoposide (10 μM) for 24 h, and cell death, as indicated by propidium iodide (5 μg/ml) uptake, determined by flow cytometry (FACSCalibur, BD Biosciences, San Jose, CA, USA). To activate Bak and induce mitochondrial outer membrane permeabilisation *in vitro*, membrane fractions from *Bak*$^{-/-}$*Bax*$^{-/-}$ MEFs expressing Bak cysteine variants were treated with 100 nM recombinant tBid for 30 min at 30°C (as described in (Dewson et al., 2008). Selected samples were treated with the functionally equivalent protein tBid^{Bax} in which the BH3 domain of Bid was substituted with the Bax BH3 domain (Hockings et al., 2015).

Cysteine accessibility to IASD labelling, one-dimensional isoelectric focussing and IASD quantification

The cysteine residue of each Bak variant was assessed for solvent exposure by incubating membrane fractions with the cysteine-labelling reagent IASD (Molecular Probes® Life Technologies, Carlsbad, CA, USA) for 30 min at 30°C (as described in (Westphal et al., 2014)). Membrane fractions were supplemented with 100 μM TCEP to prevent oxidization of cysteines that would inhibit IASD labelling. Samples were unlabelled, or incubated with IASD before, during or after tBid incubation or following denaturation with 1% w/v ASB-16 (Merck). IASD labelling was quenched by the addition of 200 mM DTT and samples solubilised in 1% ASB-16 for 10 min at 22°C. Soluble supernatant fractions were isolated by centrifugation at 16,000 ×*g* for 5 min, and added to an equal volume of IEF sample buffer (7 M urea, 2 M thiourea, 2% w/v CHAPS, Complete protease inhibitors, 4 μg/ml pepstatin A, 1% w/v ASB-16 and 0.04% w/v bromophenol blue). Samples were loaded onto 12-well Novex® pH 3-7 IEF gels (Life Technologies) and focused with a Consort EV265 power supply with increasing voltage (100 V for 1 h, 200 V for 1 h and 500 V for 30 min). IEF gels were pre-soaked in SDS buffer (75 mM Tris/HCl, pH 6.8, 0.6% w/v SDS, 15% v/v glycerol), and then transferred to PVDF membrane for western blot analysis.

IASD labelling was quantified (ImageLab 4.1, Bio-RAD) from western blots by measuring signal intensity for the unlabelled and labelled Bak band species in each lane to calculate the percentage of the total signal from each lane attributed to the faster migrating IASD-labelled species. A global background subtraction was applied to regions of interest from each western blot. Data were presented as the mean ± SD (n≥3), or range (n=2) and the number of replicates indicated on the *x*-axis. A two-tailed unpaired t-test was employed to determine significant differences ($p<0.05$) in the percentage of IASD labelled Bak before versus after tBid treatment.

Oxidant-induced disulphide linkage (CuPhe)

The cysteine residue of each Bak variant was tested for disulphide linkage with proximal cysteine residues on Bak (or other proteins) by incubation with the oxidant copper phenanthroline (CuPhe) (as per (Dewson et al., 2008)). CuPhe was prepared as a stock solution of 30 mM $CuSO_4$ and 100 mM 1,10-phenanthroline in 4:1 water/ethanol. Following incubation of membrane fractions with tBid at 30 ^{o}C, samples were pre-chilled on ice for 5 min, and then incubated with a 100-fold dilution of the CuPhe solution on ice for 15 min. Note that (Iyer et al., 2015) performed CuPhe linkage without the pre-chill incubation. Disulphide bond formation (linkage) was quenched by the addition of 20 mM N-ethyl maleimide (NEM, to label any remaining free cysteines, 10 min on ice) and 5 mM EDTA (to chelate copper, 5 min on ice) and samples analysed by non-reducing SDS PAGE or blue native PAGE (BNP).

SDS PAGE and Blue Native PAGE

CuPhe-linked samples were analysed by SDS PAGE (12% TGX gels (Life Technologies)) in the absence of reducing agents to preserve disulphide bonds. The efficiency of linkage between Bak molecules was measured by a shift in Bak migration from 1x to 2x complexes. To discriminate between linkages occurring within or between Bak dimers, CuPhe-linked samples were also analysed in tandem by blue native PAGE (BNP) to preserve the native dimer interface (i.e. the

BH3:groove interface) in addition to any disulphide bonds between Bak molecules. Migration of higher order linked complexes (i.e. greater than dimer) on BNP indicated the presence of disulphide bonds between Bak dimers. Following quenching of CuPhe with NEM and EDTA, membrane fractions were isolated by centrifugation at 16,000 ×*g* for 5 min. Supernatants were discarded and membrane pellets were solubilised in 20 mM Bis-Tris pH 7.4, 50 mM NaCl, 10% v/v glycerol, 1% w/v digitonin, and incubated on ice for 1 h and insoluble material was removed by centrifugation at 16,000 ×*g* for 5 min. The resulting supernatants were prepared for BNP by the addition of Native Sample buffer (Life Technologies) and Coomassie Additive (Life Technologies), and then loaded onto Novex® 4-16% Native PAGE 1.0 mm 10 well gels as per the manufacturer's instructions (Life Technologies). Western blot transfer to PVDF was performed at 30 V for 150 min in transfer buffer (25 mM Tris, 192 mM Glycine, 20% v/v Methanol) supplemented with 0.037 % w/v SDS. PVDF membranes were de-stained with 10% v/v acetic acid 30% v/v ethanol, then further de-stained in methanol and rinsed thoroughly with dH_2O before immunoblotting.

Immunoblotting

SDS PAGE and IEF membranes were immunoblotted for Bak using the rabbit polyclonal anti-Bak aa23-38 (B5897, Sigma-Aldrich, Castle Hill, NSW, Australia). BNP membranes were immunoblotted for Bak using an in-house anti-Bak monoclonal rat IgG (clone 7D10, WEHI, (Dewson et al., 2009, Alsop et al., 2015)), except in the case of Bak mutants ranging from G51C to P58C that were detected on BNP with the anti-Bak aa23-38. In-house monoclonal rat antibodies were used to detect recombinant Bax (clone 49-F9, WEHI), Bcl-x_L (clone 9C9, WEHI) and Mcl-1 (clone 19C 4-15, WEHI). Horseradish peroxidase conjugated IgG secondary antibodies were used; anti-rabbit (4010-05, Southern Biotech) and anti-rat (3010-05, Southern Biotech). Immobilised horseradish peroxidase was detected with Luminata Forte western HRP substrate (WBLUF0500, Millipore, Billerica, MA, USA), images captured with the ChemiDoc XRS+ System (Bio-RAD, Hercules, CA, USA) and signal intensity measured with Image Lab 4.1 software (Bio-RAD).

Blue Native PAGE densitometry

Images were transformed in Image Lab 4.1 (Bio-RAD) to correct any rotation of the image and exported as .tif for densitometry in FIJI (ImageJ 1.47n) (Schindelin et al., 2012, Schneider et al., 2012). The lookup table (LUT) was inverted and images rotated 90 degrees. Using the rectangular selection tool, a box was drawn around the lane of interest to encompass the full range of Bak signal (with fixed dimensions of 370 x 50 pixels). This box was then measured with the Dynamic ROI profiler plugin. Plot values were exported for analysis in Prism (ver 6.0f, Graphpad Software Co., La Jolla, CA, USA), and normalised to a fraction of the total intensity for each lane of interest. A clearer representation of multiple replicate plots of lane intensity was achieved by a linear rescaling of each replicate's horizontal axis so that the maximum corresponding to Bak 4x species, and the characteristic minimum (which is a highly reproducible artefact of our Bak BNP western blots) at ~720 kDa, coincided across replicates.

Simulation of linkage between dimers (V61C:V61C')

Simulation of one-dimensional arrays of Bak dimers

We considered a collection of Bak dimers in a linear arrangement, with a plane bisecting each dimer as shown in Figure 5D. Each dimer has two cysteine residues available for disulphide bonding with neighbouring dimers. We describe a link formed between cysteines on the same side of the plane as *cis* and a link that crosses the plane as *trans.* The formation of a disulphide linked oligomer is modelled by repeatedly (a) selecting an available pair of cysteines on neighbouring dimers at random, (b) declaring them linked and (c) removing those cysteines from the list of those subsequently available. In making the random selection we can apply different weights to cis and trans pairings reflected in different ratios of cis:trans linkage (as per Figure 5E). We continue until no neighbouring dimers have cysteines available for linkage, to reflect complete linkage of V61C:V61C'. We simulated closed loops consisting of varying numbers of dimers (see Figure S5).

Predicted densitometry for each Bak dimer multiplicity are presented by taking the distribution of oligomer sizes on completion of the simulation, multiplying by the number of Bak dimers in each oligomer to obtain the theoretical density that would give rise to in the western blot, using an exponential horizontal axis to mimic the nonlinear spacing of bands, and applying a gaussian kernel estimator to approximate the smearing of bands and their running into one another at higher molecular weights (see Figure S4).

Simulation of two-dimensional aggregates of Bak dimers

Here we consider a collection of Bak dimers on a two-dimensional surface (see Figure 6). Dimers are arranged on a hexagonal grid. As in the one-dimensional case each dimer has two cysteines available for disulphide linkage to a neighbouring dimer. We simulate as in the one-dimensional case, except that linkage is allowed in all directions. Results are presented as simulated western blot densitometries (as in the one-dimensional case).

Reduced linkage efficiency was modelled by introducing an edge blocking effect. Every edge between neighbouring hexagonal cells was flagged as eligible for a disulphide bond, independently at random with probability p constant across all edges in a given simulation, for p=0, 0.25, 0.5 and 0.75.

We modelled the experimental scenario where Bak dimers were formed from a mixture of equal amounts of V61C and cys-null monomers by assigning each dimer either zero, one or two available cysteines with probability 0.25, 0.5 and 0.25 respectively (see Figure S6C).

AUTHOR CONTRIBUTIONS

Conceptualization, RTU, GD, RMK; Methodology, RTU, MOH, SI, GD, RMK; Software, MOH; Investigation, RTU, SI, RB, JMB, AEA, GD; Formal analysis, RTU, MOH; Data curation, MOH;

Visualization, RTU, MOH, SI, RMK; Writing – Original Draft, RTU, RMK; Writing – Review & Editing, RTU, MOH, SI, AEA, GD, RMK; Supervision, RTU, RMK

ACKNOWLEDGMENTS

The authors declare no conflict of interest. We thank Peter Colman, Peter Czabotar, John Markham, Matthew Ritchie, Aline Oelgeklaus and Melissa Shi for critical comments on the manuscript. We thank Colin Hockings for helpful discussions regarding linear simulations. We gratefully acknowledge the IASD labelling assay development and analysis methods of Dana Westphal. Our work is supported by NHMRC grants (637337 and 1016701), and the Victorian State Government Operational Infrastructure Support and the Australian Government NHMRC IRIISS.

REFERENCES

ALSOP, A. E., FENNELL, S. C., BARTOLO, R. C., TAN, I. K., DEWSON, G. & KLUCK, R. M. 2015. Dissociation of Bak alpha1 helix from the core and latch domains is required for apoptosis. *Nat Commun,* 6**,** 6841.

ALUVILA, S. M., T. HUSTEDT, E. FAJER, P. CHOE, JY. OH, KJ. 2014. Organization of the mitochondrial apoptotic BAK pore: oligomerization of the Bak homodimers. *J Biol Chem,* 289**,** 2537-51.

BLEICKEN, S., JESCHKE, G., STEGMUELLER, C., SALVADOR-GALLEGO, R., GARCIA-SAEZ, A. J. & BORDIGNON, E. 2014. Structural model of active bax at the membrane. *Mol Cell,* 56**,** 496-505.

BROUWER, J. M., WESTPHAL, D., DEWSON, G., ROBIN, A. Y., UREN, R. T., BARTOLO, R., THOMPSON, G. V., COLMAN, P. M., KLUCK, R. M. & CZABOTAR, P. E. 2014. Bak Core and Latch Domains Separate during Activation, and Freed Core Domains Form Symmetric Homodimers. *Mol Cell,* 55**,** 938-46.

CHEN, F. Y., LEE, M. T. & HUANG, H. W. 2003. Evidence for membrane thinning effect as the mechanism for peptide-induced pore formation. *Biophys J,* 84**,** 3751-8.

CHEN, L., WILLIS, S. N., WEI, A., SMITH, B. J., FLETCHER, J. I., HINDS, M. G., COLMAN, P. M., DAY, C. L., ADAMS, J. M. & HUANG, D. C. 2005. Differential targeting of prosurvival Bcl-2 proteins by their BH3-only ligands allows complementary apoptotic function. *Molecular Cell,* 17**,** 393-403.

CHENG, E. H., SHEIKO, T. V., FISHER, J. K., CRAIGEN, W. J. & KORSMEYER, S. J. 2003. VDAC2 inhibits BAK activation and mitochondrial apoptosis. *Science,* 301**,** 513-517.

CZABOTAR, P. E., WESTPHAL, D., DEWSON, G., MA, S., HOCKINGS, C., FAIRLIE, W. D., LEE, E. F., YAO, S., ROBIN, A. Y., SMITH, B. J., HUANG, D. C., KLUCK, R. M., ADAMS, J. M. & COLMAN, P. M. 2013. Bax Crystal Structures Reveal How BH3 Domains Activate Bax and Nucleate Its Oligomerization to Induce Apoptosis. *Cell,* 152**,** 519-31.

DAI, H., SMITH, A., MENG, X. W., SCHNEIDER, P. A., PANG, Y. P. & KAUFMANN, S. H. 2011. Transient binding of an activator BH3 domain to the Bak BH3-binding groove initiates Bak oligomerization. *J Cell Biol,* 194**,** 39-48.

DEWSON, G., KRATINA, T., CZABOTAR, P., DAY, C. L., ADAMS, J. M. & KLUCK, R. M. 2009. Bak activation for apoptosis involves oligomerization of dimers via their alpha6 helices. *Mol Cell,* 36**,** 696-703.

DEWSON, G., KRATINA, T., SIM, H. W., PUTHALAKATH, H., ADAMS, J. M., COLMAN, P. M. & KLUCK, R. M. 2008. To trigger apoptosis Bak exposes its BH3 domain and homo-dimerizes via BH3:grooove interactions. *Mol Cell,* 30**,** 369-380.

DEWSON, G., MA, S., FREDERICK, P., HOCKINGS, C., TAN, I., KRATINA, T. & KLUCK, R. M. 2012. Bax dimerizes via a symmetric BH3:groove interface during apoptosis. *Cell Death Differ,* 19**,** 661-70.

DU, H., WOLF, J., SCHAFER, B., MOLDOVEANU, T., CHIPUK, J. E. & KUWANA, T. 2011. BH3 domains other than Bim and Bid can directly activate Bax/Bak. *J Biol Chem,* 286**,** 491-501.

FERRER, P. E., FREDERICK, P., GULBIS, J. M., DEWSON, G. & KLUCK, R. M. 2012. Translocation of a Bak C-terminus mutant from cytosol to mitochondria to mediate cytochrome C release: implications for Bak and Bax apoptotic function. *PLoS One,* 7**,** e31510.

GAHL, R. F., HE, Y., YU, S. & TJANDRA, N. 2014. Conformational rearrangements in the pro-apoptotic protein, Bax, as it inserts into mitochondria: a cellular death switch. *J Biol Chem,* 289**,** 32871-82.

GAVATHIOTIS, E., REYNA, D. E., DAVIS, M. L., BIRD, G. H. & WALENSKY, L. D. 2010. BH3-Triggered Structural Reorganization Drives the Activation of Proapoptotic BAX. *Molecular Cell,* 40**,** 481-92.

GEORGE, N. M., EVANS, J. J. & LUO, X. 2007. A three-helix homo-oligomerization domain containing BH3 and BH1 is responsible for the apoptotic activity of Bax. *Genes Dev,* 21**,** 1937-1948.

GILBERT, R. J. 2016. Protein-lipid interactions and non-lamellar lipidic structures in membrane pore formation and membrane fusion. *Biochim Biophys Acta,* 1858**,** 487-99.

GRIFFITHS, G. J., DUBREZ, L., MORGAN, C. P., JONES, N. A., WHITEHOUSE, J., CORFE, B. M., DIVE, C. & HICKMAN, J. A. 1999. Cell damage-induced conformational changes of the pro-apoptotic protein Bak in vivo precede the onset of apoptosis. *Journal of Cell Biology,* 144**,** 903-914.

GROSSE, L., WURM, C. A., BRUSER, C., NEUMANN, D., JANS, D. C. & JAKOBS, S. 2016. Bax assembles into large ring-like structures remodeling the mitochondrial outer membrane in apoptosis. *EMBO J,* 35**,** 402-13.

GRUNDLING, A., BLASI, U. & YOUNG, R. 2000. Biochemical and genetic evidence for three transmembrane domains in the class I holin, lambda S. *J Biol Chem,* 275**,** 769-76.

HOCKINGS, C., ANWARI, K., NINNIS, R. L., BROUWER, J., O'HELY, M., EVANGELISTA, M., HINDS, M. G., CZABOTAR, P. E., LEE, E. F., FAIRLIE, W. D., DEWSON, G. & KLUCK, R. M. 2015. Bid chimeras indicate that most BH3-only proteins can directly activate Bak and Bax, and show no preference for Bak versus Bax. *Cell Death Dis,* 6**,** e1735.

IYER, S., BELL, F., WESTPHAL, D., ANWARI, K., GULBIS, J., SMITH, B. J., DEWSON, G. & KLUCK, R. M. 2015. Bak apoptotic pores involve a flexible C-terminal region and juxtaposition of the C-terminal transmembrane domains. *Cell Death Differ*.

KLUCK, R. M., ESPOSTI, M. D., PERKINS, G., RENKEN, C., KUWANA, T., BOSSY-WETZEL, E., GOLDBERG, M., ALLEN, T., BARBER, M. J., GREEN, D. R. & NEWMEYER, D. D. 1999. The pro-apoptotic proteins, Bid and Bax, cause a limited permeabilization of the mitochondrial outer membrane that is enhanced by cytosol. *J Cell Biol,* 147**,** 809-22.

KUWANA, T., OLSON, N. H., KIOSSES, W. B., PETERS, B. & NEWMEYER, D. D. 2016. Pro-apoptotic Bax molecules densely populate the edges of membrane pores. *Sci Rep,* 6**,** 27299.

LAZAROU, M., STOJANOVSKI, D., FRAZIER, A. E., KOTEVSKI, A., DEWSON, G., CRAIGEN, W. J., KLUCK, R. M., VAUX, D. L. & RYAN, M. T. 2010. Inhibition of Bak activation by VDAC2 is dependent on the Bak transmembrane anchor. *J Biol Chem,* 285**,** 36876-83.

LEE, E. F., GRABOW, S., CHAPPAZ, S., DEWSON, G., HOCKINGS, C., KLUCK, R. M., GRAY, D. H., WITKOWSKI, M. T., EVANGELISTA, M., PETTIKIRIARACHCHI, A., BOUILLET, P., CORY, S., VANDENBERG, C. J., LANE, R. M., CZABOTAR, P. E., COLMAN, P. M., SMITH, B. J., KILE, B. T. & FAIRLIE, W. D. 2016. Physiological restraint of Bak by Bcl-xL is essential for cell survival. *Genes Dev,* In press.

LEE, M. T., SUN, T. L., HUNG, W. C. & HUANG, H. W. 2013. Process of inducing pores in membranes by melittin. *Proc Natl Acad Sci U S A,* 110**,** 14243-8.

LESHCHINER, E. S., BRAUN, C. R., BIRD, G. H. & WALENSKY, L. D. 2013. Direct activation of full-length proapoptotic BAK. *Proc Natl Acad Sci U S A,* 110**,** E986-95.

LINDSTEN, T., ROSS, A. J., KING, A., ZONG, W., RATHMELL, J. C., SHIELS, H. A., ULRICH, E., WAYMIRE, K. G., MAHAR, P., FRAUWIRTH, K., CHEN, Y., WEI, M., ENG, V. M., ADELMAN, D. M., SIMON, M. C., MA, A., GOLDEN, J. A., EVAN, G., KORSMEYER, S. J., MACGREGOR, G. R. & THOMPSON, C. B. 2000. The combined functions of proapoptotic Bcl-2 family members Bak and Bax are essential for normal development of multiple tissues. *Mol Cell,* 6**,** 1389-1399.

LLAMBI, F., MOLDOVEANU, T., TAIT, S. W., BOUCHIER-HAYES, L., TEMIROV, J., MCCORMICK, L. L., DILLON, C. P. & GREEN, D. R. 2011. A unified model of mammalian BCL-2 protein family interactions at the mitochondria. *Mol Cell,* 44**,** 517-31.

LUO, L., YANG, J. & LIU, D. 2014. Integration and oligomerization of Bax protein in lipid bilayers characterized by single molecule fluorescence study. *J Biol Chem,* 289**,** 31708-18.

MA, S., HOCKINGS, C., ANWARI, K., KRATINA, T., FENNELL, S., LAZAROU, M., RYAN, M. T., KLUCK, R. M. & DEWSON, G. 2013. Assembly of the Bak apoptotic pore: a critical role for the Bak protein alpha6 helix in the multimerization of homodimers during apoptosis. *J Biol Chem,* 288**,** 26027-38.

MA, S. B., NGUYEN, T. N., TAN, I., NINNIS, R., IYER, S., STROUD, D. A., MENARD, M., KLUCK, R. M., RYAN, M. T. & DEWSON, G. 2014. Bax targets mitochondria by distinct mechanisms before or during apoptotic cell death: a requirement for VDAC2 or Bak for efficient Bax apoptotic function. *Cell Death Differ*.

MOLDOVEANU, T., LIU, Q., TOCILJ, A., WATSON, M. H., SHORE, G. & GEHRING, K. 2006. The x-ray structure of a BAK homodimer reveals an inhibitory zinc binding site. *Molecular Cell,* 24**,** 677-688.

MUELLER, M., GRAUSCHOPF, U., MAIER, T., GLOCKSHUBER, R. & BAN, N. 2009. The structure of a cytolytic alpha-helical toxin pore reveals its assembly mechanism. *Nature,* 459**,** 726-30.

NASU, Y., BENKE, A., ARAKAWA, S., YOSHIDA, G. J., KAWAMURA, G., MANLEY, S., SHIMIZU, S. & OZAWA, T. 2016. In Situ Characterization of Bak Clusters Responsible for Cell Death Using Single Molecule Localization Microscopy. *Sci Rep,* 6**,** 27505.

NECHUSHTAN, A., SMITH, C. L., LAMENSDORF, I., YOON, S. H. & YOULE, R. J. 2001. Bax and Bak coalesce into novel mitochondria-associated clusters during apoptosis. *Journal of Cell Biology,* 153**,** 1265-1276.

PANG, Y. P., DAI, H., SMITH, A., MENG, X. W., SCHNEIDER, P. A. & KAUFMANN, S. H. 2012. Bak Conformational Changes Induced by Ligand Binding: Insight into BH3 Domain Binding and Bak Homo-Oligomerization. *Sci Rep,* 2**,** 257.

SALVADOR-GALLEGO, R., MUND, M., COSENTINO, K., SCHNEIDER, J., UNSAY, J., SCHRAERMEYER, U., ENGELHARDT, J., RIES, J. & GARCIA-SAEZ, A. J. 2016. Bax assembly into rings and arcs in apoptotic mitochondria is linked to membrane pores. *EMBO J,* 35**,** 389-401.

SATSOURA, D., KUCERKA, N., SHIVAKUMAR, S., PENCER, J., GRIFFITHS, C., LEBER, B., ANDREWS, D. W., KATSARAS, J. & FRADIN, C. 2012. Interaction of the full-length Bax protein with biomimetic mitochondrial liposomes: a small-angle neutron scattering and fluorescence study. *Biochim Biophys Acta,* 1818**,** 384-401.

SCHINDELIN, J., ARGANDA-CARRERAS, I., FRISE, E., KAYNIG, V., LONGAIR, M., PIETZSCH, T., PREIBISCH, S., RUEDEN, C., SAALFELD, S., SCHMID, B., TINEVEZ, J. Y., WHITE, D. J., HARTENSTEIN, V., ELICEIRI, K., TOMANCAK, P. & CARDONA, A. 2012. Fiji: an open-source platform for biological-image analysis. *Nat Methods,* 9**,** 676-82.

SCHNEIDER, C. A., RASBAND, W. S. & ELICEIRI, K. W. 2012. NIH Image to ImageJ: 25 years of image analysis. *Nat Methods,* 9**,** 671-5.

SONG, L., HOBAUGH, M. R., SHUSTAK, C., CHELEY, S., BAYLEY, H. & GOUAUX, J. E. 1996. Structure of staphylococcal alpha-hemolysin, a heptameric transmembrane pore. *Science,* 274**,** 1859-66.

SUBBURAJ, Y., COSENTINO, K., AXMANN, M., PEDRUEZA-VILLALMANZO, E., HERMANN, E., BLEICKEN, S., SPATZ, J. & GARCIA-SAEZ, A. J. 2015. Bax monomers form dimer units in the membrane that further self-assemble into multiple oligomeric species. *Nat Commun,* 6**,** 8042.

SUNG, T. C., LI, C. Y., LAI, Y. C., HUNG, C. L., SHIH, O., YEH, Y. Q., JENG, U. S. & CHIANG, Y. W. 2015. Solution Structure of Apoptotic BAX Oligomer: Oligomerization Likely Precedes Membrane Insertion. *Structure,* 23**,** 1878-88.

SUZUKI, M., YOULE, R. J. & TJANDRA, N. 2000. Structure of Bax: coregulation of dimer formation and intracellular localization. *Cell,* 103**,** 645-654.

TRAN, V. H., BARTOLO, R., WESTPHAL, D., ALSOP, A., DEWSON, G. & KLUCK, R. M. 2013. Bak apoptotic function is not directly regulated by phosphorylation. *Cell Death Dis,* 4**,** e452.

WEBER, K., HARPER, N., SCHWABE, J. & COHEN, G. M. 2013. BIM-mediated membrane insertion of the BAK pore domain is an essential requirement for apoptosis. *Cell Rep,* 5**,** 409-20.

WEI, M. C., ZONG, W. X., CHENG, E. H., LINDSTEN, T., PANOUTSAKOPOULOU, V., ROSS, A. J., ROTH, K. A., MACGREGOR, G. R., THOMPSON, C. B. & KORSMEYER, S. J. 2001. Proapoptotic BAX and BAK: a requisite gateway to mitochondrial dysfunction and death. *Science,* 292**,** 727-730.

WESTPHAL, D., DEWSON, G., MENARD, M., FREDERICK, P., IYER, S., BARTOLO, R., GIBSON, L., CZABOTAR, P. E., SMITH, B. J., ADAMS, J. M. & KLUCK, R. M. 2014. Apoptotic pore formation is associated with in-plane insertion of Bak or Bax central helices into the mitochondrial outer membrane. *Proc Natl Acad Sci U S A,* 111**,** E4076-85.

WOLTER, K. G., HSU, Y. T., SMITH, C. L., NECHUSHTAN, A., XI, X. G. & YOULE, R. J. 1997. Movement of Bax from the cytosol to mitochondria during apoptosis. *Journal of Cell Biology,* 139**,** 1281-1292.

ZHANG, Z., SUBRAMANIAM, S., KALE, J., LIAO, C., HUANG, B., BRAHMBHATT, H., CONDON, S. G., LAPOLLA, S. M., HAYS, F. A., DING, J., HE, F., ZHANG, X. C., LI, J., SENES, A., ANDREWS, D. W. & LIN, J. 2016. BH3-in-groove dimerization initiates and helix 9 dimerization expands Bax pore assembly in membranes. *EMBO J,* 35**,** 208-36.

ZHANG, Z., ZHU, W., LAPOLLA, S. M., MIAO, Y., SHAO, Y., FALCONE, M., BOREHAM, D., MCFARLANE, N., DING, J., JOHNSON, A. E., ZHANG, X. C., ANDREWS, D. W. & LIN, J. 2010. Bax forms an oligomer via separate, yet interdependent, surfaces. *J Biol Chem,* 285**,** 17614-17627.

ZHOU, L. & CHANG, D. C. 2008. Dynamics and structure of the Bax-Bak complex responsible for releasing mitochondrial proteins during apoptosis. *J Cell Sci,* 121**,** 2186-96.

Figure 1

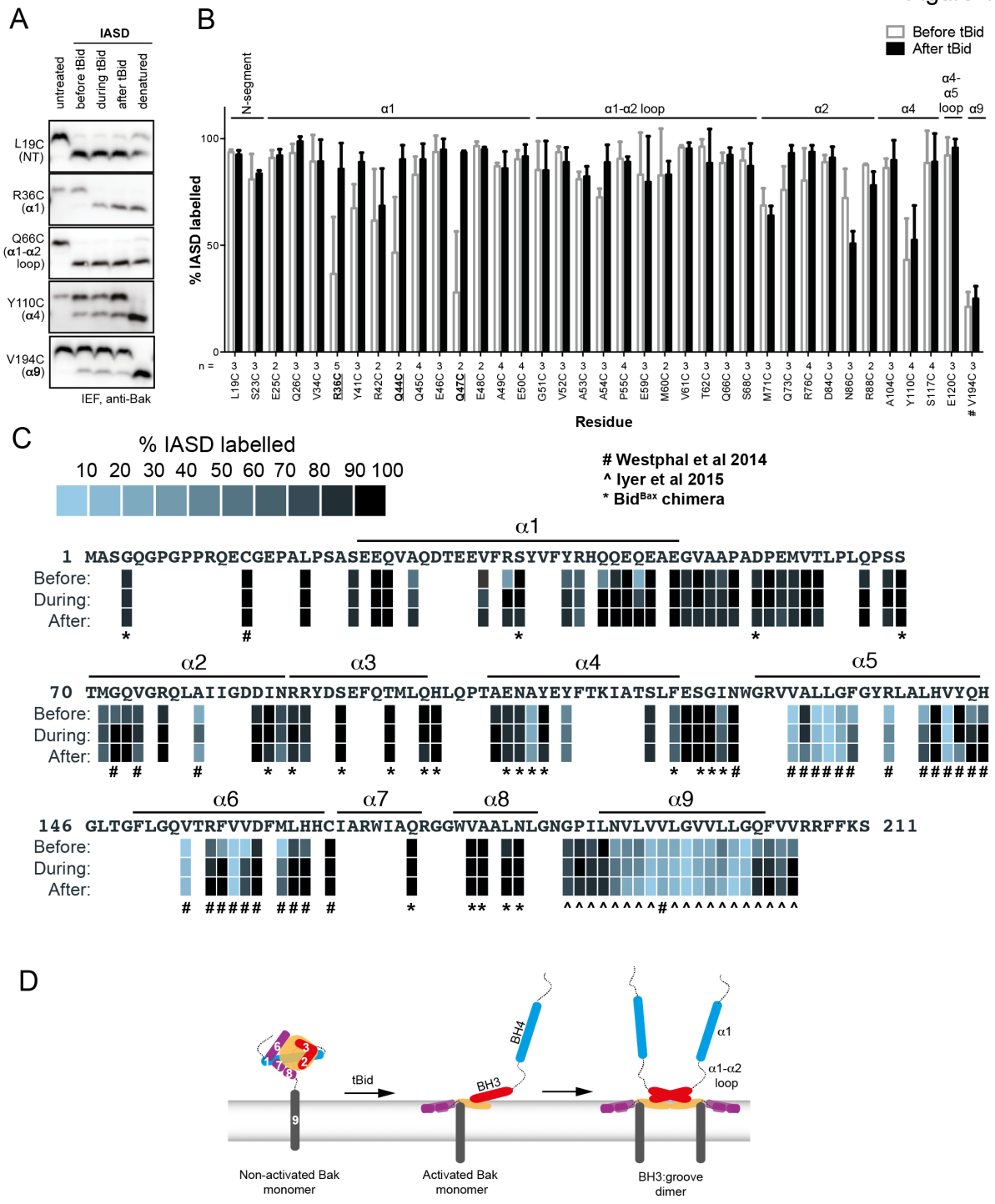
A
IASD
untreated
before tBid
during tBid
after tBid
denatured
L19C (NT)
R36C (α1)
Q66C (α1-α2 loop)
Y110C (α4)
V194C (α9)
IEF, anti-Bak
B
Before tBid
After tBid
N-segment
α1
α1-α2 loop
α2
α4
α4-α5 loop
α9
% IASD labelled
Residue
C
% IASD labelled
10 20 30 40 50 60 70 80 90 100
Westphal et al 2014
^ Iyer et al 2015
* Bid^Bax chimera
α1
1 MASGQGPGPPRQECGEPALPSASEEQVAQDTEEVFRSYVFYRHQQEQEAEGVAAPADPEMVTLPLQPSS
Before:
During:
After:
α2
α3
α4
α5
70 TMGQVGRQLAIIGDDINRRYDSEFQTMLQHLQPTAENAYEYFTKIATSLFESGINWGRVVALLGFGYRLALHVYQH
α6
α7
α8
α9
146 GLTGFLGQVTRFVVDFMLHHCIARWIAQRGGWVAALNLGNGPILNVLVVLGVVLLGQFVVRRFFKS 211
D
tBid
BH4
BH3
α1
α1-α2 loop
Non-activated Bak monomer
Activated Bak monomer
BH3:groove dimer

Figure 1 Following oligomerization, the Bak N-segment, α1 and α1-α2 loop become fully solvent-exposed in contrast to the partially exposed core (α2-α5) and latch (α6-α9).

(A) Solvent exposure of hBak cysteine mutants was assessed by IASD labelling before (lane 2), during (lane 3) and after (lane 4) treatment with tBid. Controls of unlabelled (untreated, lane 1) and fully labelled (denatured, lane 5) Bak were included for comparison. Example IEF western blots are shown.

(B) Quantitation of IASD labelling before and after treatment with tBid for the panel of previously untested Bak residues. Data are mean ± SD (n≥3), or range (n=2), with n for each residue labelled on the x-axis. IASD labelling data for residue V194C were from (Westphal et al., 2014) (denoted #). Residues for which there is a significant difference in IASD labelling before versus after tBid are in bold and underlined ($p<0.05$).

(C) Heat map overview of Bak IASD labelling with tBid treatment from (B) pooled with published analyses from (Westphal et al., 2014)(denoted #) or (Iyer et al., 2015)(denoted ^) and from treatment with the $tBid^{Bax}$ chimera (denoted *; see also Figure S2).

(D) Schematic of Bak structural rearrangement from its non-activated monomeric state to the activated dimer. Helices are numbered for the non-activated Bak. Note the complete solvent-exposure of α1 and the α1-α2 loop in the activated dimer.

Figure 2

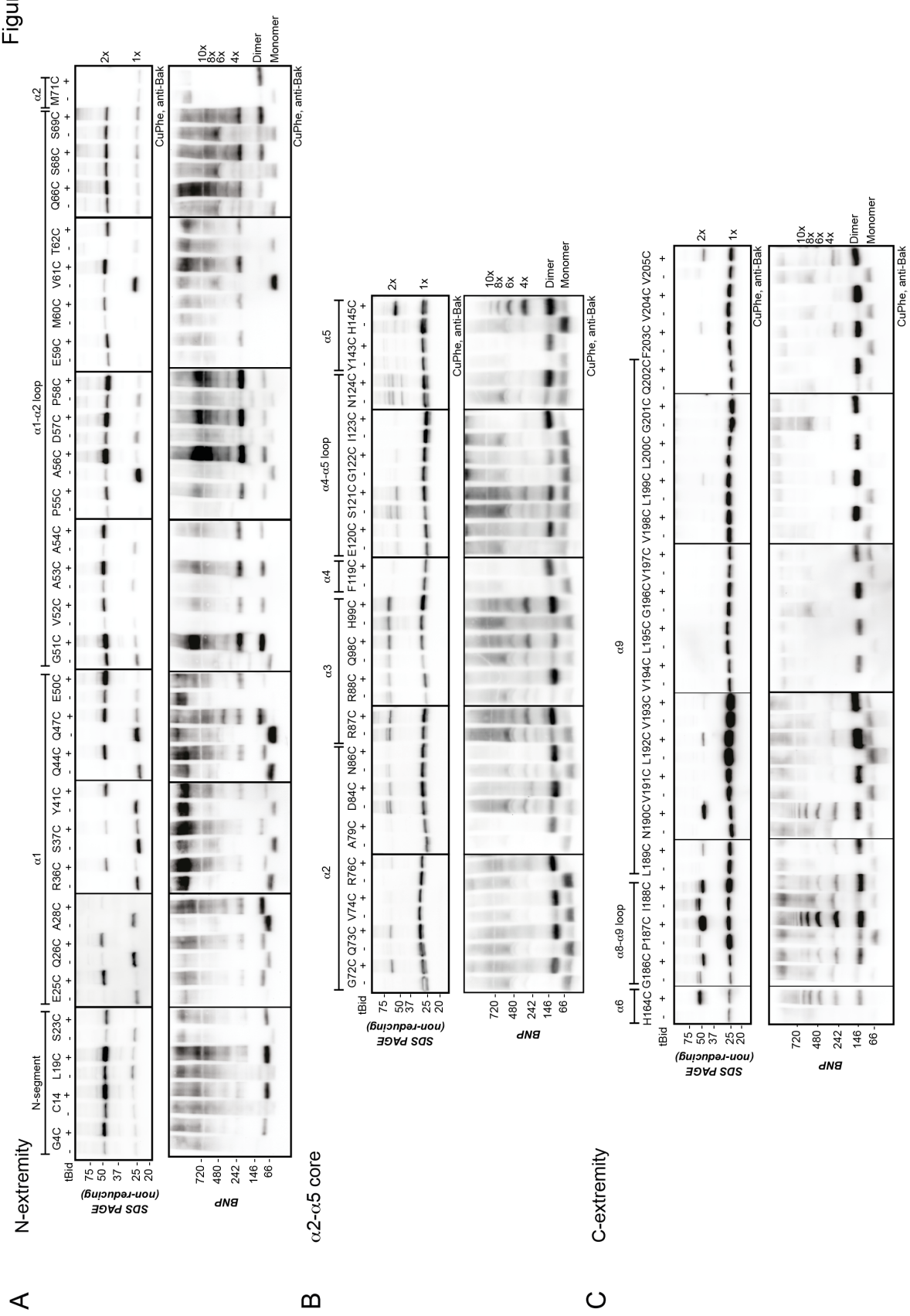
A
N-extremity
N-segment
α1
α1-α2 loop
α2
G4C C14 L19C S23C E25C Q26C A28C R36C S37C Y41C Q44C Q47C E50C G51C V52C A53C A54C P55C A56C D57C P58C E59C M60C V61C T62C Q66C S68C S69C M71C
tBid
SDS PAGE (non-reducing)
BNP
2x
1x
10x
8x
6x
4x
Dimer
Monomer
CuPhe, anti-Bak
B
α2-α5 core
α2
α3
α4
α4-α5 loop
α5
G72C Q73C V74C R76C A79C D84C N86C R87C R88C Q98C H99C F119C E120C S121C G122C I123C N124C Y143C H145C
C
C-extremity
α6
α8-α9 loop
α9
H164C G186C P187C I188C L189C N190C V191C L192C V193C V194C L195C G196C V197C V198C L199C L200C G201C Q202C F203C V204C V205C

Figure 2 The N- and C-extremities of oligomerized Bak are mobile relative to the α2-α5 core dimer. Mitochondrial fractions from cells expressing the indicated Bak cysteine mutants were incubated with tBid to oligomerize Bak, and oxidant (CuPhe) added to induce disulphide bonds. Aliquots were analyzed by non-reducing SDS PAGE (upper panels) and BNP (lower panels), and immunoblotted for Bak to detect linked species.

(A) Cysteine linkage occurs throughout the N-extremity.

(B) Cysteine linkage occurs, but is less complete, in the α2-α5 dimer core.

(C) Cysteine linkage occurs in the C-extremity. (See also α6:α6 linkage in (Dewson et al., 2008) and α9:α9 linkage in (Iyer et al., 2015)).

Figure 3

A

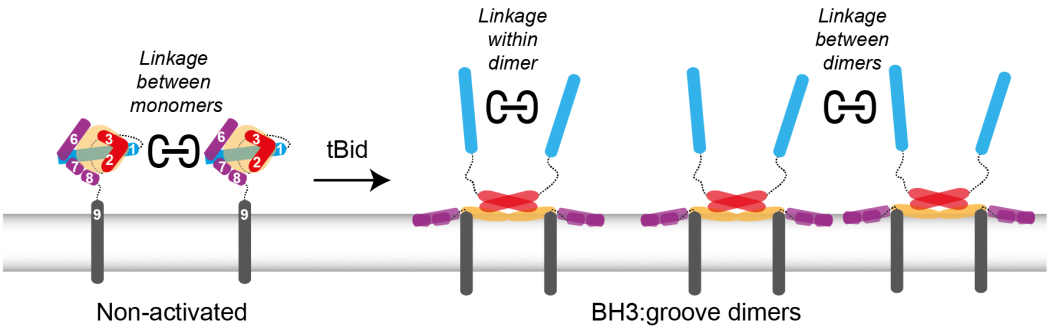

B

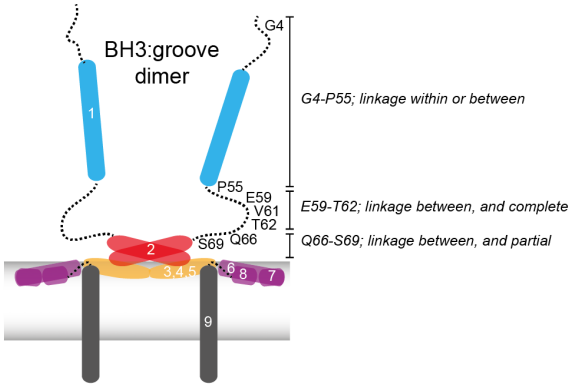

C

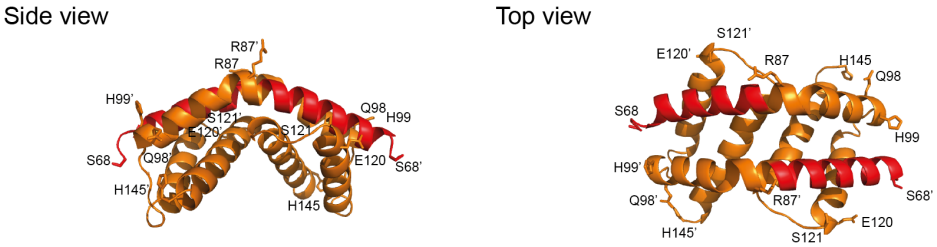

D

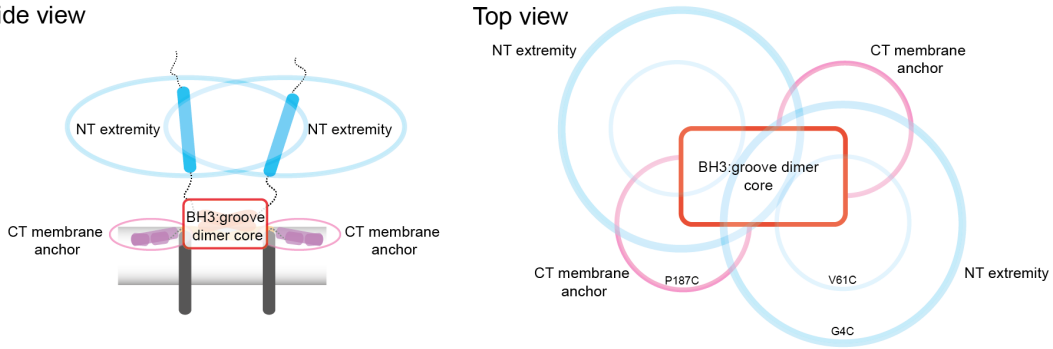

E

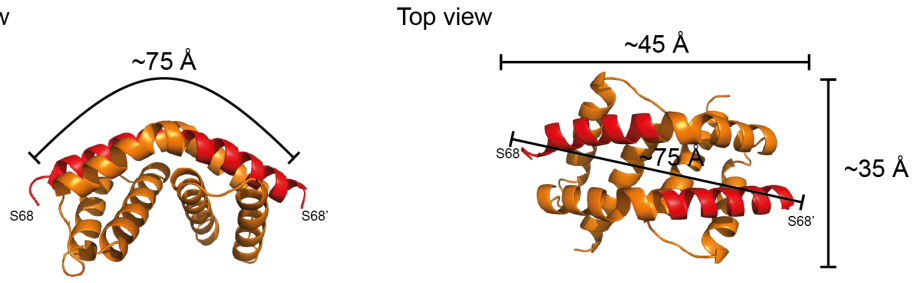

Figure 3 Linkage constraints for different regions of the active Bak dimer support a flexible extremity model for full-length Bak dimers in the MOM.

(A) The oxidant CuPhe induces linkage *between* Bak monomers or dimers, or *within* Bak dimers. Correlation of BNP with non-reducing SDS PAGE can differentiate linkage within and between dimers.

(B) Summary of linkage outcomes within or between dimers for residues in the Bak dimer N-extremity.

(C) Linkage at the lateral corners of the Bak α2-α5 core dimer is highlighted with residue labels and sticks on the crystal structure (4U2V (Brouwer et al., 2014)).

(D) Schematic of the activated Bak dimer at the membrane in side and top views. The range of movement of the N- and C-extremities is indicated with coloured ovals (blue and pink respectively).

(E) Our linkage data are consistent with the dimensions of the Bak core dimer. The dimensions of the Bak α2-α5 core dimer 4U2V (Brouwer et al., 2014) are shown in side view and top view. In the crystal structure, the distance from one edge of the core at S68 over the bended structure of the symmetric core to the opposing S68' is ~75 Å. Thus, for residues in the mobile N-extremity to link within the core dimer, the two homotypic cysteine residues must bridge a distance of ~75 Å. This is not feasible for the residue V61C which is ~30 Å from the symmetric core.

Figure 4

A

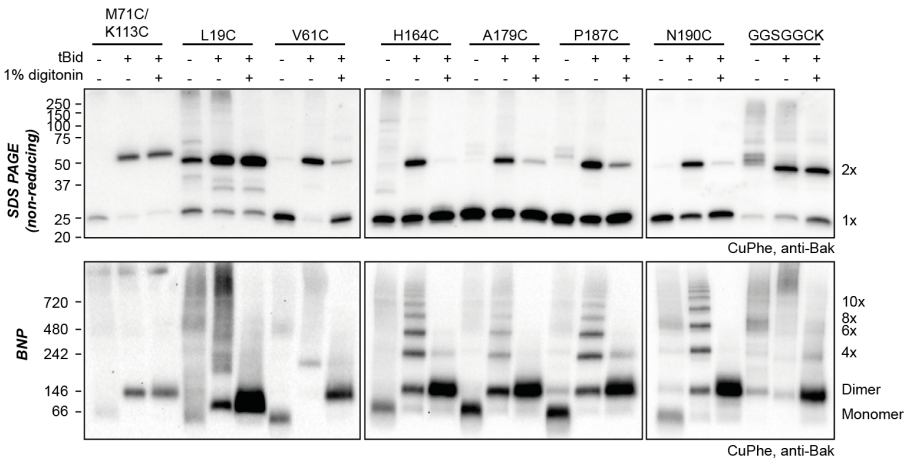
M71C/ K113C
L19C
V61C
H164C
A179C
P187C
N190C
GGSGGCK
tBid
1% digitonin
SDS PAGE (non-reducing)
250
150
100
75
50
37
25
20
2x
1x
CuPhe, anti-Bak
BNP
720
480
242
146
66
10x
8x
6x
4x
Dimer
Monomer
CuPhe, anti-Bak

B

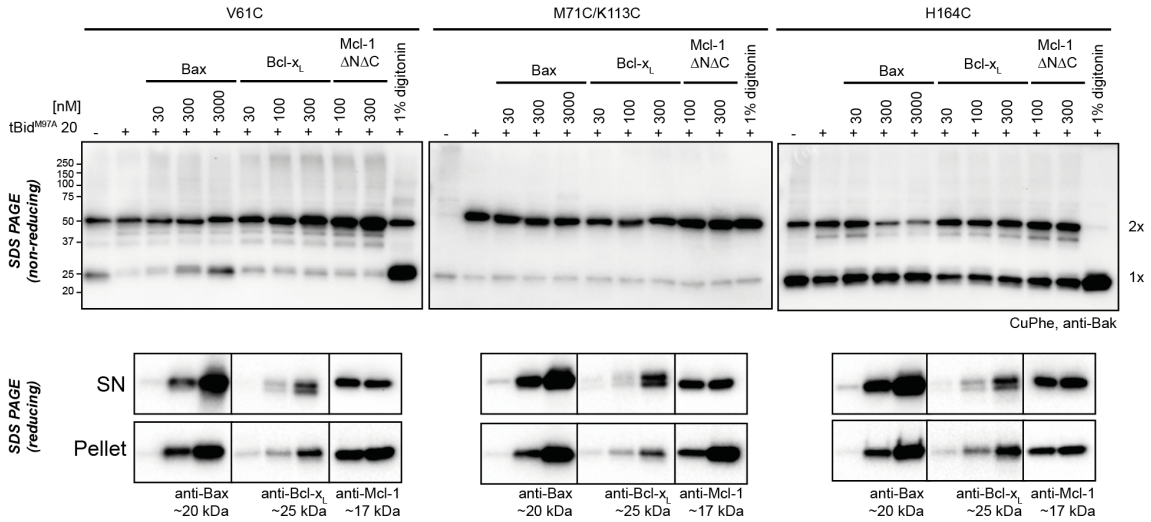
V61C
M71C/K113C
H164C
Bax
Bcl-xL
Mcl-1 ΔNΔC
1% digitonin
[nM]
tBidM97A 20
SDS PAGE (non-reducing)
2x
1x
CuPhe, anti-Bak
SDS PAGE (reducing)
SN
Pellet
anti-Bax ~20 kDa
anti-Bcl-xL ~25 kDa
anti-Mcl-1 ~17 kDa

Figure 4 Bak dimer-dimer interactions are disrupted by detergent or Bax.

(A) Digitonin prevents linkage between Bak dimers. Membrane fractions expressing the indicated Bak single-cysteine variants were first treated with tBid, and then supplemented, as indicated, with detergent (1% digitonin) prior to cysteine linkage. Two additional mutants were included to show linkage within dimers at the BH3:groove interface (M71C/K113C) and at extensions to the C-terminus (GGSGGCK).

(B) Bax can disrupt Bak dimer-dimer association. Membrane fractions first treated with $tBid^{M97A}$ were then incubated, as indicated, with Bax, Bcl-x_L, Mcl-1ΔN151ΔC23 or digitonin prior to cysteine linkage (upper panels). Supernatant and pellet fractions showed partial translocation of each recombinant protein to the membrane fraction (lower panels).

Figure 5

A

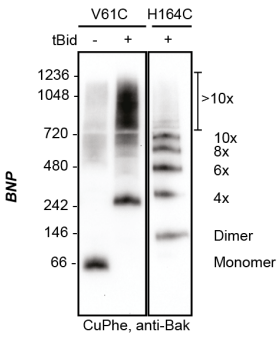

B

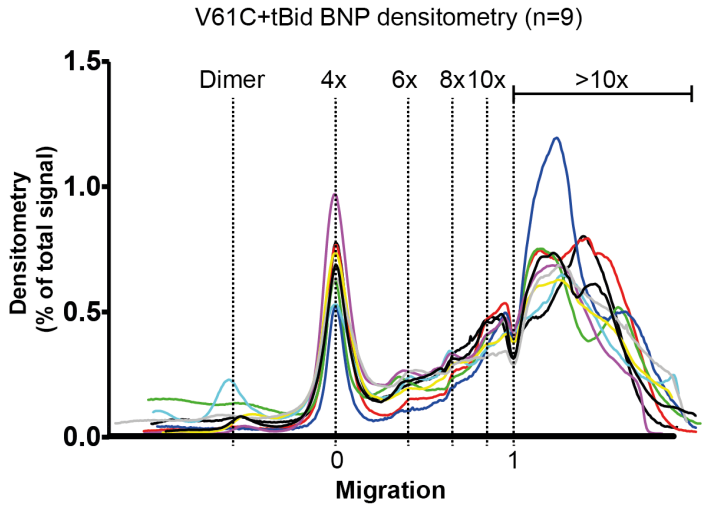

C

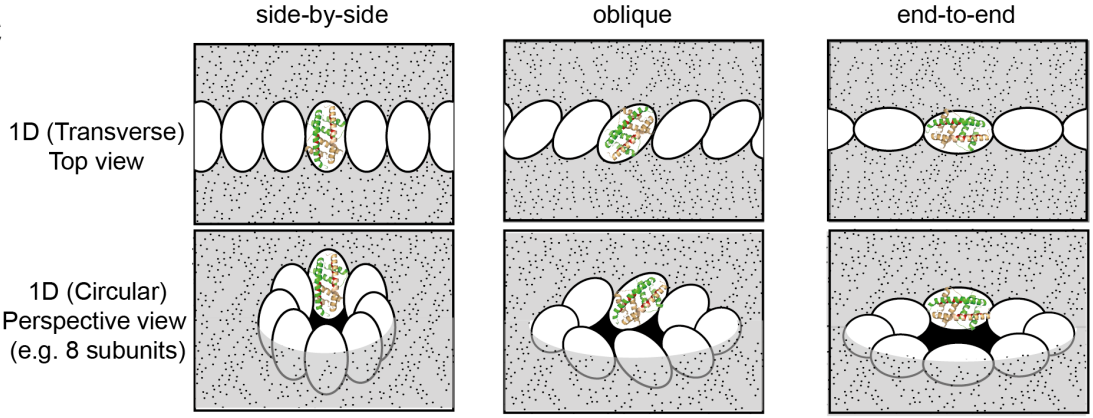

D

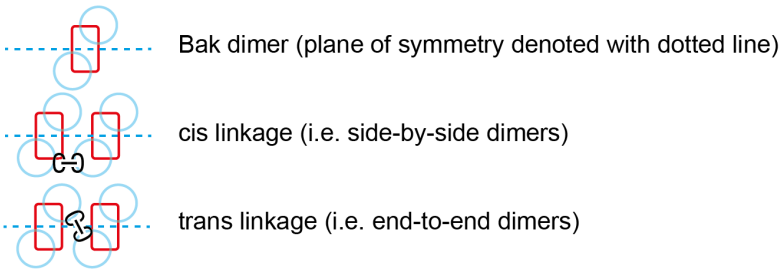

E

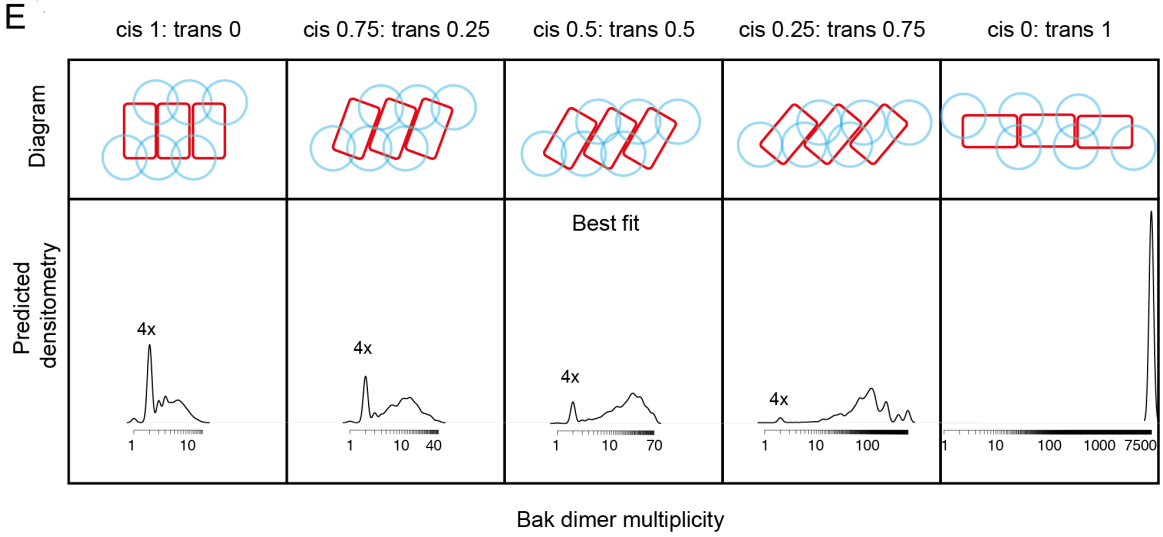

Figure 5 Bak dimer arrangement examined by one-dimensional stochastic simulations: rules out a side-by-side or an end-to-end arrangement of Bak dimers

(A) V61C:V61C' linkage is a marker of dimer-dimer interaction. BNP analysis of V61C:V61C' linkage revealed no dimers, and a high proportion of 4x and >10x species. In contrast, H164C:H164C' linkage revealed a ladder of linked species.

(B) Densitometry of V61C:V61C' BNP linkage in Bak oligomers shows negligible dimers but reproducible linked species at 4x, 6x, 8x, and 10x, and a large population of species >10x. Densitometry data (n=9) were normalised to the area under the curve after alignment as described in Experimental Procedures. To correct for small variations in electrophoretic migration, we employed a noise reduction algorithm in which the 4x peak (0) and a minima at ~720 kDa (1) were aligned between replicates.

(C) Models of Bak dimers arranging linearly via symmetric protein-protein interfaces to extend across the membrane surface (upper, transverse) or line a circular pore (lower, circular). Side-by-side, end-to-end and oblique arrangements are illustrated. Each white oval represents the Bak dimer core, and flexible extremities are not illustrated. Although the simulations in (E) employed a closed loop of 10,000 dimers, an arbitrary number of dimer subunits are shown in each illustration.

(D) Each Bak dimer is bisected by a plane of symmetry. Links that form between dimers on the same side of the plane are denoted *cis*, and links between dimers that cross the plane are denoted *trans*.

(E) Simulation of Bak dimers in a linear array shows no preference for *cis* or *trans* linkage between dimers. Bak dimers in a linear array, ranging from side-by-side to end-to-end together with intermediate oblique arrangements that would result from different *cis-trans* linkage ratios are illustrated (top panel). Simulated predicted densitometries for several cis:trans ratios, with a maximum of 10,000 dimers (displaying the average of 100 replicate simulations), are shown (lower panel). Note that cis 0.5: trans 0.5 gives the best agreement with the V61C:V61C' BNP linkage data, consistent with an oblique array of dimers. Other maximum oligomer sizes (comprising 6, 10, 20 or 50 dimers) were also simulated (Figure S5).

Figure 6

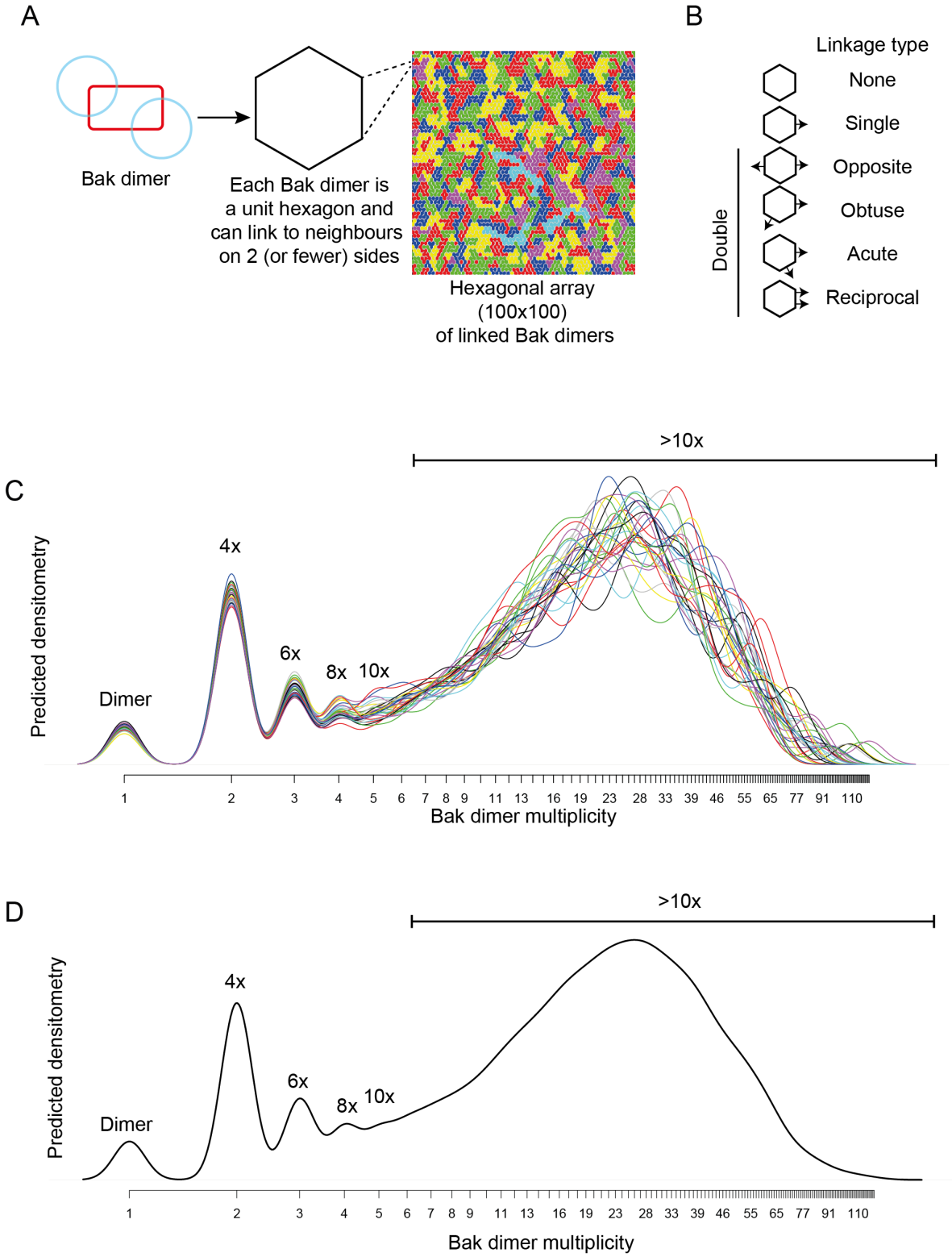
A
Bak dimer
Each Bak dimer is
a unit hexagon and
can link to neighbours
on 2 (or fewer) sides
Hexagonal array
(100x100)
of linked Bak dimers
B
Linkage type
None
Single
Opposite
Obtuse
Acute
Reciprocal
Double
C
>10x
Predicted densitometry
Dimer
4x
6x
8x
10x
1 2 3 4 5 6 7 8 9 11 13 16 19 23 28 33 39 46 55 65 77 91 110
Bak dimer multiplicity
D
>10x
Predicted densitometry
Dimer
4x
6x
8x
10x
1 2 3 4 5 6 7 8 9 11 13 16 19 23 28 33 39 46 55 65 77 91 110
Bak dimer multiplicity

Figure 6 Bak dimer arrangement examined by two-dimensional stochastic simulations: a random arrangement is the best fit for the V61C:V61C' BNP linkage densitometry.

(A) A grid of 100x100 was designated for the 2D simulations. Each unit hexagon within that grid represented a Bak dimer, with the capacity to link to 2 neighbouring hexagons. The direction of linkage from each hexagon was randomised. An example visual output from a 100x100 hexagonal array is shown: neighbouring subsets of linked Bak dimers within the grid are delineated by different colours.

(B) Linkage possibilities between each dimer unit in a hexagonal 2D array.

(C,D) Overlay (C), and average (D) of 30 predicted densitometry plots.

Figure 7

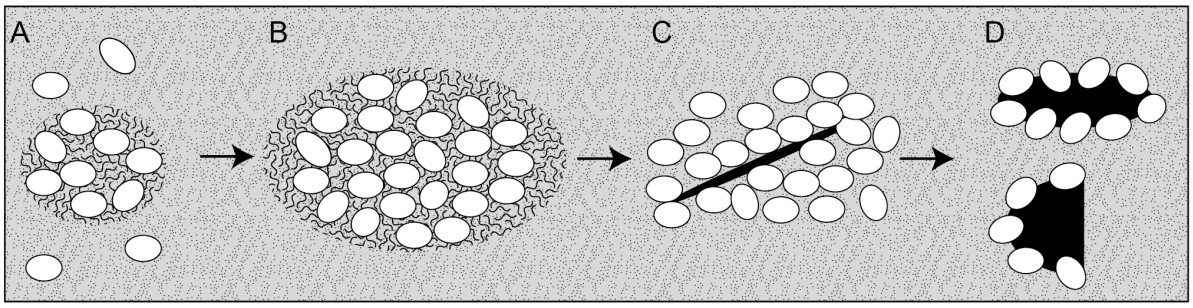

Figure 7 Bak dimers aggregate in compact, disordered clusters to disrupt the mitochondrial outer membrane.

(A) Upon activation, Bak dimers penetrate the outer leaflet of the membrane and accumulate in a compact, irregular cluster.

(B) More dimers converge on the cluster, thus enlarging the patch of membrane disturbance.

(C) Once the patch attains a critical threshold area the membrane bilayer is ruptured, relieving membrane tension.

(D) Lipids and Bak dimers rearrange to bury exposed hydrophobic surfaces, yielding a variety of protein-lipid (toroidal) channels or "pores". Our assays survey a mixture of Bak linkage products derived from stages (B), (C) and (D).

SUPPLEMENTAL INFORMATION

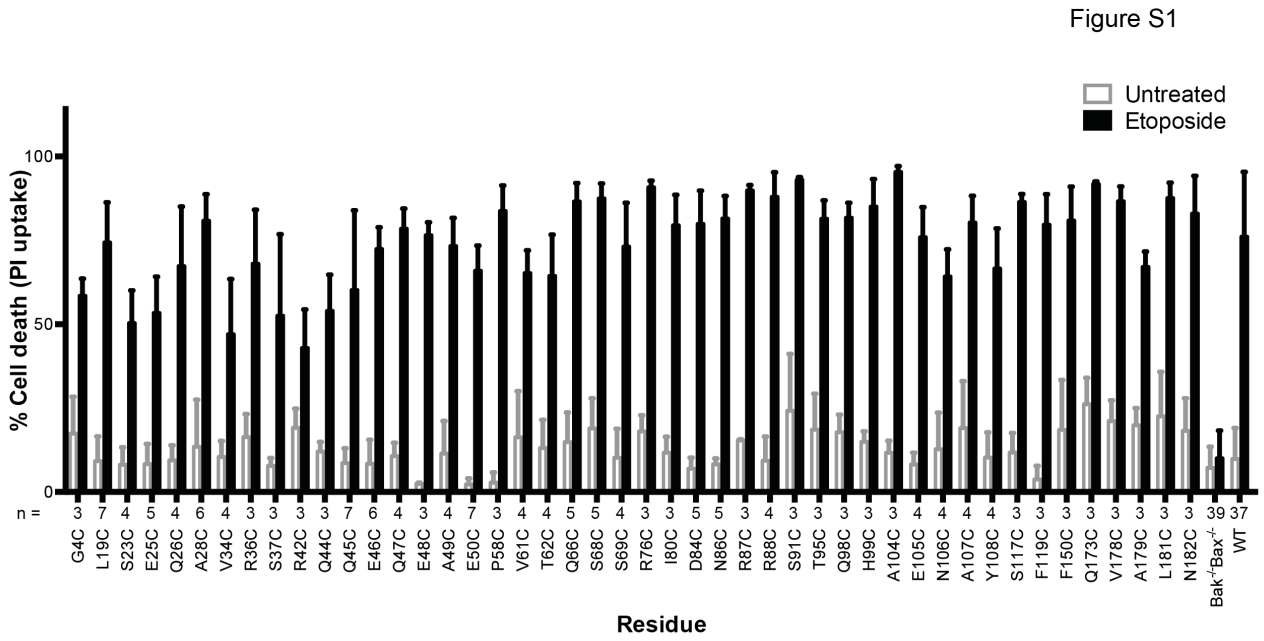

Figure S1 Bak cysteine variants retain apoptotic function. *Bak*$^{-/-}$*Bax*$^{-/-}$ MEF expressing Bak cysteine variants were treated with 10 μM etoposide for 24 h and the percentage cell death quantified by propidium iodide uptake. Data are for unpublished mutants only and are the mean ± SD. The number of replicates (n) for each residue is labelled on the x-axis.

Figure S2

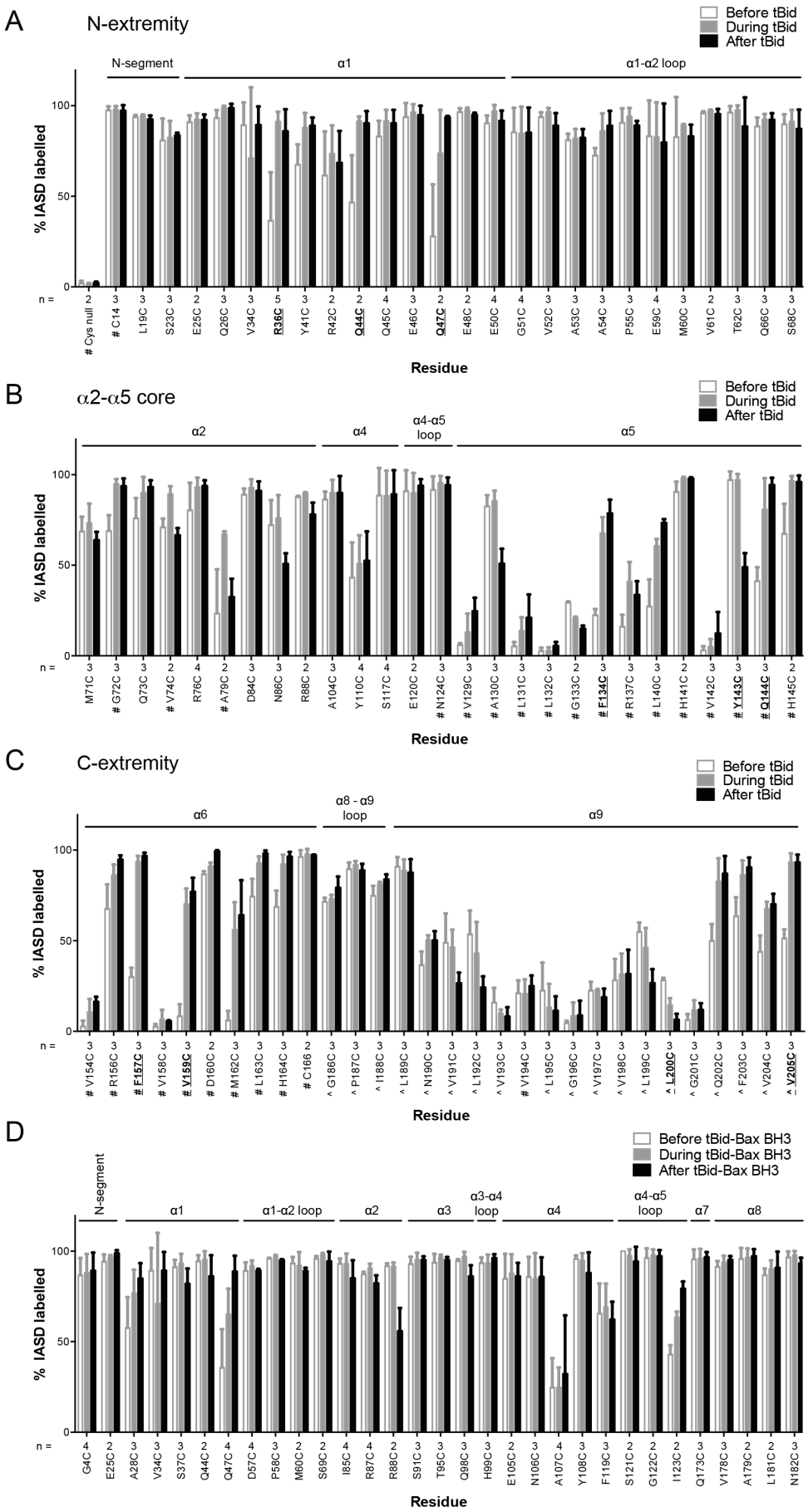
A
N-extremity
Before tBid
During tBid
After tBid
N-segment
α1
α1-α2 loop
% IASD labelled
Residue
B
α2-α5 core
α2
α4
α4-α5 loop
α5
C
C-extremity
α6
α8 - α9 loop
α9
D
Before tBid-Bax BH3
During tBid-Bax BH3
After tBid-Bax BH3
α2
α3
α3-α4 loop
α4
α4-α5 loop
α7
α8

Figure S2 Quantitation of Bak IASD labelling before, during and after Bak activation.

(A,B,C). Labelling before, during or after treatment with tBid, segregated by Bak N-extremity (A), Core (B), and C-extremity (C). Previously untested Bak residues have been pooled with data from previous studies (# denotes data from (Westphal et al., 2014), ^ denotes data from (Iyer et al., 2015)). Data are mean ± SD, or range (n=2), with n for each residue labelled on the x-axis. Residues for which there is a significant difference in IASD labelling before versus after tBid are in bold and underlined ($p<0.05$).

(D) IASD labelling for selected Bak variants before, during and after treatment with $tBid^{Bax}$ chimera (Hockings et al., 2015). Data are mean ± SD ($n \geq 3$), or range (n=2), with n for each residue labelled on the x-axis. No significant differences (p value cutoff of 0.05) in IASD labelling before versus after $tBid^{Bax}$ were observed.

Figure S3

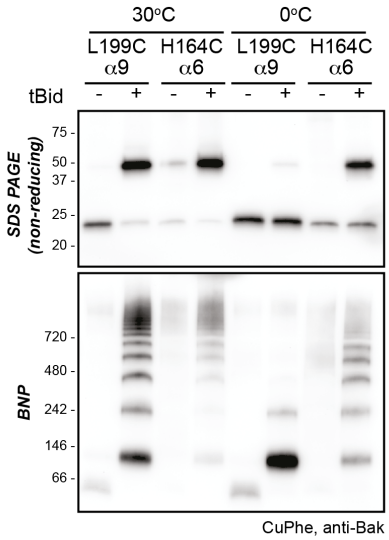

Figure S3 Higher temperature enhances disulphide bonding of cysteine residues in α6 (H164C) and the α9 transmembrane domain (L199C). Mitochondrial fractions from cells expressing the indicated Bak cysteine mutants were incubated with tBid to oligomerize Bak, and oxidant (CuPhe) added to induce disulphide bonds. Samples were incubated with CuPhe for 15 min either at 0°C or at 30°C. Aliquots were analyzed by non-reducing SDS PAGE (upper) and BNP (lower), and immunoblotted for Bak to detect linked species. Note that linkage outside the membrane (H164C:H164C') was efficient even at 0°C.

Figure S4

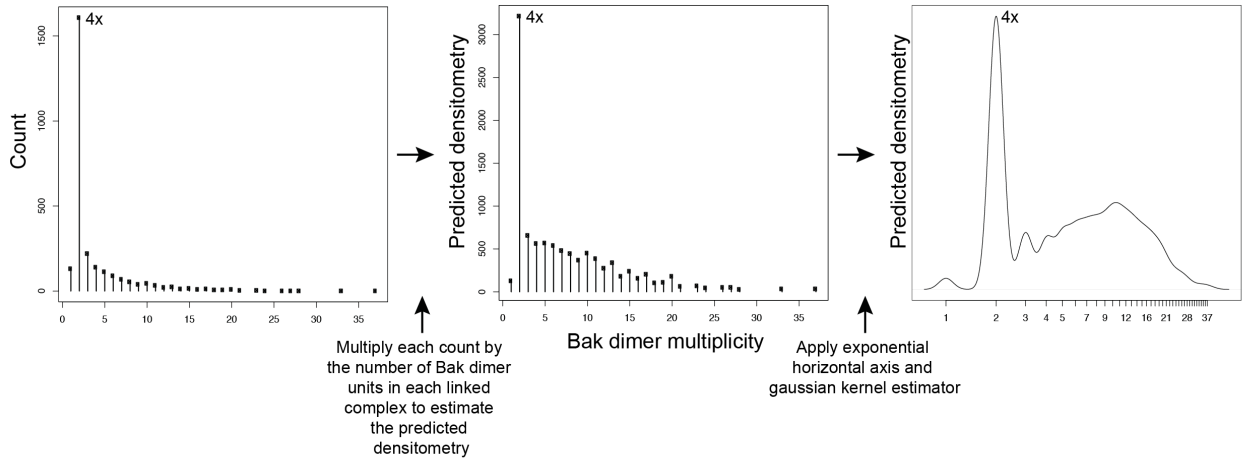

Figure S4 Adjustment to simulation output to allow qualitative comparison to western blot data. Mathematical simulations of Bak dimer linkage generated frequency distributions of the size of Bak complexes (multiples of Bak dimers). These frequency distributions were then transformed to a predicted densitometry by multiplying each count by the number of Bak dimer units present in each linked Bak complex. For instance, the count representing 2x complexes, is multiplied by 1, the count representing 4x complexes is multiplied by 2, the count representing 6x complexes is multiplied by 3, etc. This predicted densitometry approximates the total relative abundance of Bak molecules in each linked Bak complex, which was then transformed with an exponential horizontal axis to mimic the nonlinear spacing of bands, and a gaussian kernel estimator to approximate the smearing of bands (especially at higher molecular weights) to allow qualitative comparison to western blot densitometry outputs.

Figure S5

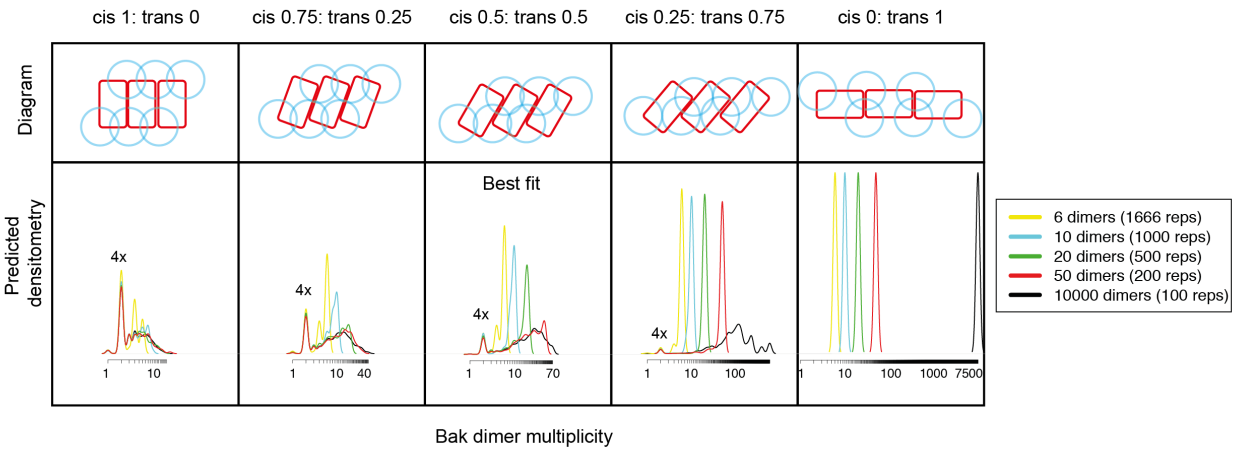

Figure S5 Larger oligomer sizes (i.e. 10,000 or 50 dimers) in 1D simulations are the best fit for linkage of V61C:V61C'. Simulated predicted densitometries for several cis:trans ratios in the 1D model are shown, with maximum oligomer sizes of 10,000 dimers (black, see also Figure 5E), 50 dimers (red), 20 dimers (green), 10 dimers (light blue) and 6 dimers (yellow). Note that the V61C:V61C' linkage (Figure 5B) generated prominent complexes greater than 10x which do not arise with simulated maximum oligomer sizes of 10 or fewer dimers. The average of replicate simulations is shown, and the number of replicates indicated in the figure legend. A ratio of cis 0.5:trans 0.5 and oligomer sizes of 10,000 and 50 dimers were qualitatively the best fit for the V61C linkage data, suggesting that aggregates comprising 20 Bak dimers or less are not a major component in our mitochondrial system if we assume all Bak dimers are in a linear array.

Figure S6

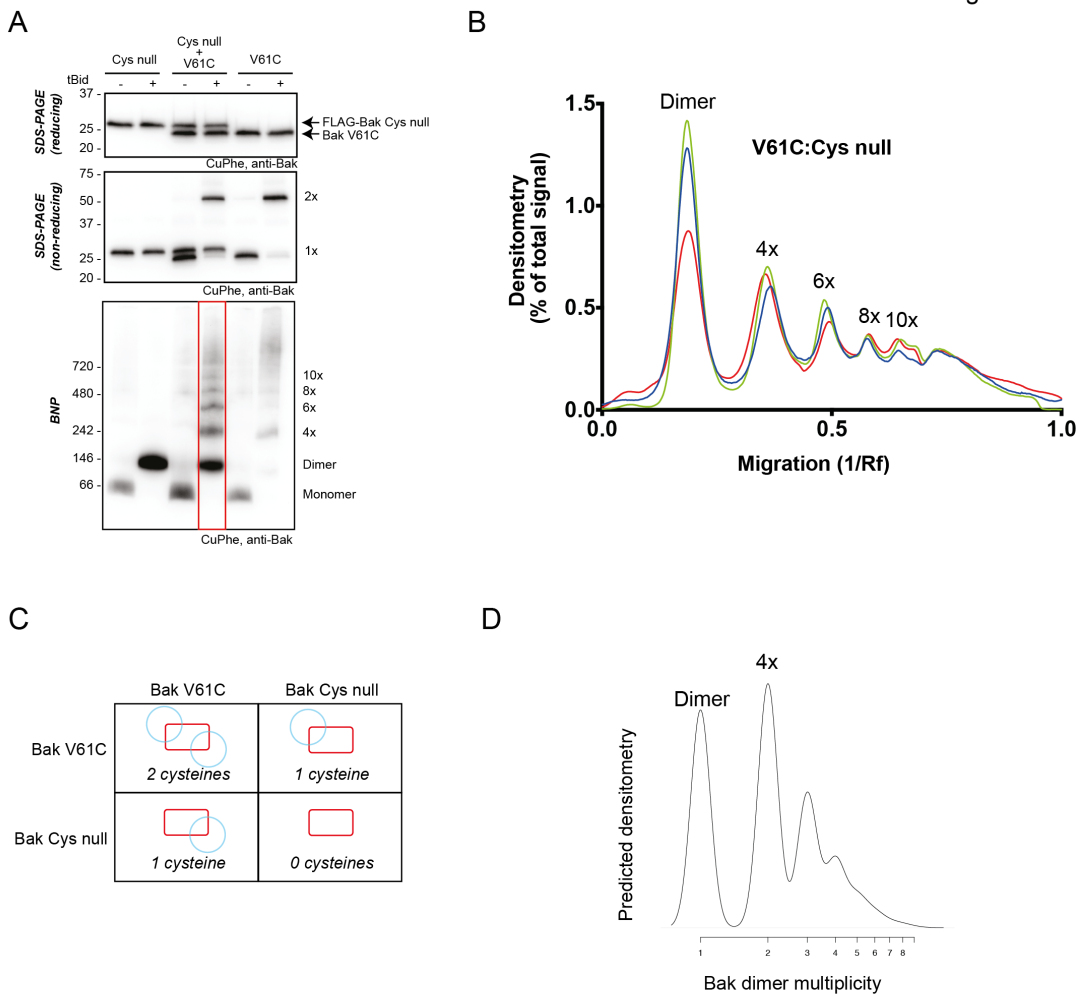

Figure S6 2D simulation with reduced efficiency linkage successfully models reduced linkage in mitochondrial experiments.

(A) Co-expression of Bak V61C with Bak Cys null resulted in less high order linkage species on BNP. Membrane fractions expressing Bak V61C, FLAG-Cys null, or both, were incubated with or without tBid, and then subjected to CuPhe linkage and analysis by BNP, non-reducing SDS PAGE or reducing SDS PAGE.

(B) Densitometry of BNP linkage data following tBid treatment for 3 replicates of the V61C:Flag-Cys null co-expression. Data are normalised to the area under the curve.

(C) Diagram showing the four types of dimers that would form upon co-expression of V61C and Cys null variants of Bak (i.e. a system in which 50 % of Bak molecules are unable to link). Note that dimers will be capable of 0, 1 or 2 linkages.

(D) The 2D simulation was altered to incorporate 50% linkage-incompetent Bak molecules. This simulation yielded a good concordance with the V61C:Flag Cys null densitometry.

Figure S7

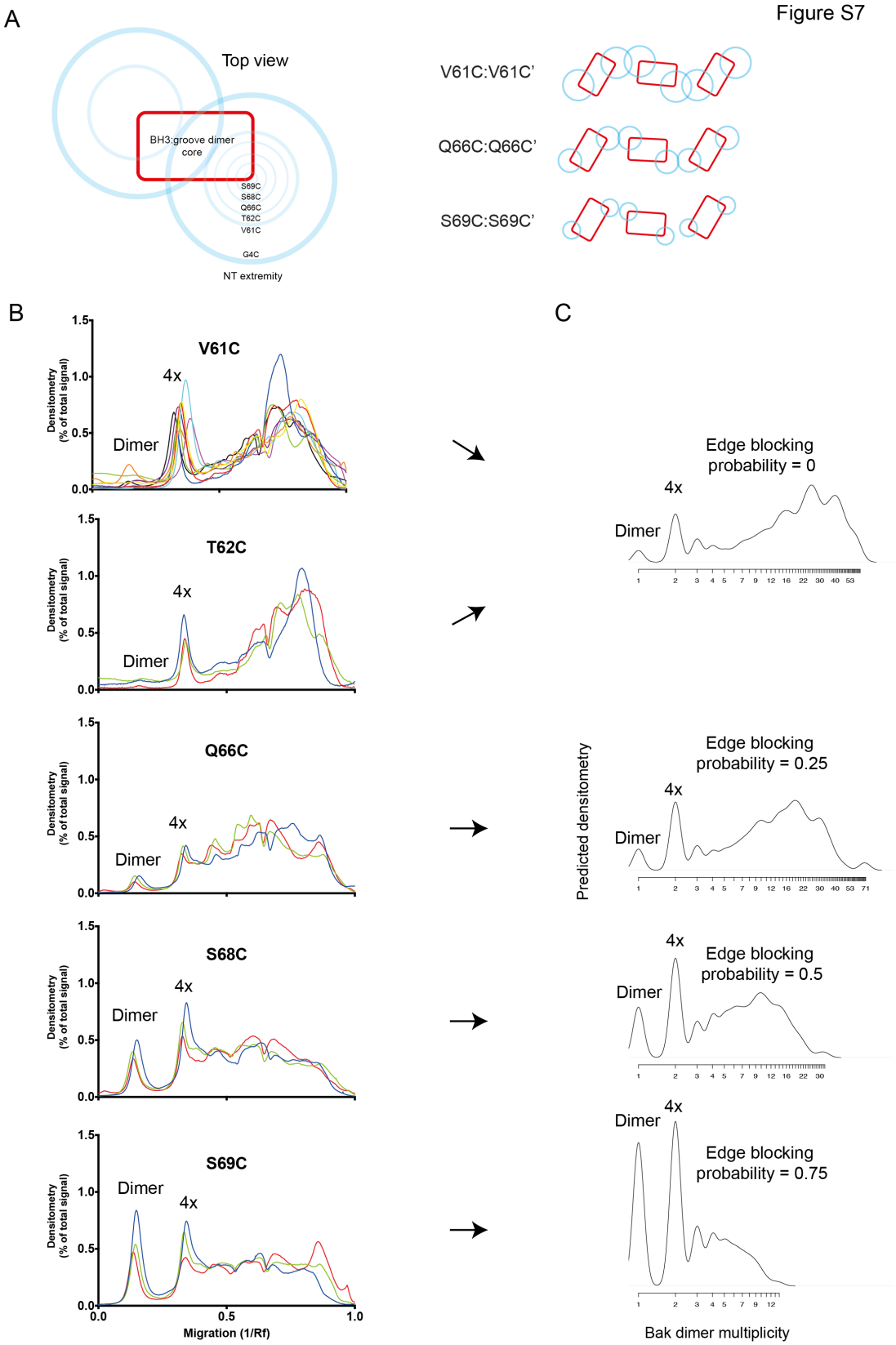
A
Top view
BH3:groove dimer core
S69C
S68C
Q66C
T62C
V61C
G4C
NT extremity
V61C:V61C'
Q66C:Q66C'
S69C:S69C'
B
C
V61C
T62C
Q66C
S68C
S69C
4x
Dimer
Densitometry (% of total signal)
Migration (1/Rf)
Predicted densitometry
Edge blocking probability = 0
Edge blocking probability = 0.25
Edge blocking probability = 0.5
Edge blocking probability = 0.75
Bak dimer multiplicity

Figure S7 2D simulation with edge blocking probability successfully models mitochondrial experiments in which Bak linkage becomes constrained as cysteines are positioned closer to the dimer core.

(A) Residues between V61C and the core of the Bak dimer have a progressively more limited range of movement. On the left, blue circles are shown on a schematic of the Bak dimer to represent the range of movement for G4C, V61C, T62C, Q66C, S68C and S69C. On the right, an illustration of the reduced overlap of Bak dimer extremities (blue circles) is shown for residues with progressively smaller ranges of movement (e.g. V61C>Q66C>S69C).

(B) Densitometry of BNP outputs from V61C, T62C, Q66C, S68C and S69C highlight the reduced linkage efficiency (relative to V61C) as cysteine substitutions approach the constrained core of the Bak dimer.

(C) The 2D simulation was altered to incorporate an "edge blocking probability" to mimic the increasing linkage constraint experienced by cysteine substitutions as they approached the core. The best approximation of each cysteine substitution mutant is indicated by arrows.